MASTERARBEIT / MASTER´S THESIS

Titel der Masterarbeit / Title of the Master´s Thesis

„Analysis of the histone epi-proteome in glioma cells“

verfasst von / submitted by

Nele Feldmann, BSc

angestrebter akademischer Grad / in partial fulfilment of the requirements for the degree of

Master of Science (MSc)

Wien, 2019 / Vienna 2019

Studienkennzahl lt. Studienblatt / degree programme code as it appears on the student record sheet:	A 066 863
Studienrichtung lt. Studienblatt / degree programme as it appears on the student record sheet:	Masterstudium Biologische Chemie / Biological Chemistry (Master)
Betreut von / Supervisor:	Univ.-Prof. Dipl.-Chem. Dr. Lothar Brecker

Acknowledgment

Science knows no country, because knowledge belongs to humanity, and is the torch which illuminates the world.

- *Louis Pasteur* -

Hereby I want to thank Dr. Christian Feller and Dr. Tobias Weiss for their support during the project, for providing the opportunity to learn and to work independently.

I also thank Prof. Lothar Brecker for being my formal supervisor and his kind support during the process of writing.

And thanks to my lab partner Marcel Bühler for creating a great work environment.

Furthermore, I´m beyond grateful for my family who always bolstered me up.
And Sebastian, thank you for being my bastion of calm.

Table of content

Index of figures

Index of tables

Abbreviations

ACN	acetonitrile
ChIP-seq	chromatin immunoprecipitation sequencing
CoV	coefficient of variation
DIA-PRM	Data independent acquisition-parallel reaction monotoring
FDA	Food and Drug Administration
GBM	glioblastoma multiforme
GIC/GSC	glioma-initiating cell/ glioma stem cell
H3K9	lysine 9 on histone 3
HDAC	histone deacetylases
KDM/HDM	histone (lysine) demethylase
KMT/HMT	histone (lysine) methyltransferase
MS	mass spectrometry
ncRNA	non-coding RNA
PRC2	Polycomb repressive complex 2
PTM	post-translational modification
TFA	trifluoroacetic acid
2-HG	2-hydroxyglutarate

Summary

Gene expression and the arrangement of chromatin structure in marmmalian cells is regulated by epigenetic mechanisms such as post-translational modifications of histones. Therefore the investigation on the modification system plays a crucial role in the understanding of epigenetic processes.

The methods of choice to investigate on PTMs are antibody-based and include immunoblotting, immunohistochemistry and ChIP-seq. But a limiting circumstance is the availability of antibodies: they are act only against few of the reported histone modifications and sequence isoforms [1].

The aim of this project was to identify changes in the abundance of >100 histones after treatment with small molecule inhibitors that inhibit specific epigenetic modifiers.

Using a recently developed mass spectrometry-based approach we were able to study the function and regulation of the inhibited epigenetic enzymes.

The obtained results show that histone epi-proteomics provide a new strategy, especially in combination with other approaches, to create a link between epigenetic changes and the development of a disease.

Introduction

Chromatin and histone post-translationale modifications

The genetic blueprint of multicellular organisms is organised within the DNA. To keep all the processes in the body operating the given information has to be converted into functional products. Subsequently, these substances dictate cell function.
Changes in gene expression are studied by the rising field of epigenetics. Epigenetic changes are regular and natural but are also influenced by factors such as age, lifestyle, environment and disease state. DNA-Methylation, histone modification and non-coding RNA-associated gene silencing are the three systems that initiate and sustain these processes.
In this project we focused on histone modifications.

The genetic information is packed within the DNA that is wrapped around protein complexes, the so called histones. These two units form a nucleosome. Every nucleosome consists of the DNA superhelix which is wrapped around the histone. There are two copies of every histone (H2A, H2B, H3, H4). Another histone (H1) serves as a linker connecting the other histones. This structure allows a tight packaging of the DNA within the nucleus. The histones are predominantly globular with the exception of their N-terminals, which are unstructured. Due to their expositional state these „tails“ provide the opportunity of modification such as methylation, phosphorylation or acetylation.

Histone lysine methylation, for example, plays a role in cell function such as heterochromatin formation, DNA repair, cell fate determination and X chromosome inactivation [2].

Despite the „writers“ that mark histone residues with a functional group, the „erasers“ that remove these residues and restore the initial state, the recognition and interpretation of the histone modifications is done by specific enzymes called „readers“.

A common modification is the methylation of lysine 4 of histone 3 (H3K4), that is associated with transcriptionally active genes [3].

In 2001, Jenuwein et al. suggested that not just a single histone modification but the combination of them reveals a „histone code“ that led to the activation or inactivation of genes [4]. For example, the phosphorylation of serine 10 on histone 3 that provides the ability of the acetylation of lysine 14 on histone 3 by Gcn5 [5]. The trimethylation of lysine 4 on histone 3 is another example. The trimethylated state is associated with transcriptionally activity whereas the di- and trimethylation of lysine 9 on histone 3 (H3K9me2/3) led to the repression of transcription [6]. A study in which histone modifications in context with muscle stem cell ageing were examined, showed that different modification patterns, so called „motifs“, can be observed [7].

Cancer epigenetics

The specific characteristic of cancer is either induced through DNA mutations that alter the functions of produced proteins or by epigenetics processes. Therefore, the previous described modifications of histones lead to a different modification pattern as in healthy organisms.

There is a growing interest in the investigation of the epigenetic mechanisms and how it´s possible to connect epigenetic alterations with different classes of tumors. Although changes in DNA methylation are long known to be involved in the development of cancer [8] the complexity of the histone PTM´s represent a major challenge but also a promising chance when it comes to novel cancer treatment methods.

Consequently, a great amount of inhibitors have been developed.

One of a well-known change in histone modification in respect of some malignancies is a global reduction of acetylation on H4K16ac. This reduction is induced by the overexpression of histone deacetylases [9].

Glioblastoma is the most malignant form of the most common malignant primary brain tumor (WHO grade 4). Displaying the aggressivity of the tumor, the median survival ranging from 14 to 30 month [10].

Different epigenetic regulator genes have already been identified as the driving force in the development of gliomas. IDH1/IDH2 mutations are the most

characteristic ones in lower grade gliomas whereas changes in the DNA methylation pattern along with histone 3 mutations occur in pediatric high grade gliomas [11].

Being able to classify subgroups of gliomas via epigenetic markers is a big advantage when it comes to treatment decision. Genome-wide DNA methylation profile is one of these biomarkers [12].

In regard of the earlier mentioned IDH mutations a gain-of-function causes a neo-enzymatic activity that is responsible for an accumulation of the onco-metabolite 2-hyroxyglutarate. This lead, by interefering global chromatin organization, to an expression of oncogenes [13].

Therefore, there is a growing interest not just in the scientific academia but in the pharmaceutical industry to find a way to inhibit cancer-related modifications by using small molecule-based inhibitors. Limited by poor understanding of the cellular mode of action of the histone modification system, the risk of off-target effects is highly increased. Thus, makes it difficult in regard to optimal dose and treatment time of such inhibitors.

Getting knowledge about the cellular mode of action of the epigenetically active compounds via the histone epi-proteome is a promising approach, which maybe generate a path to a personalized treatment of a disease.

Aims of the project

The aim of my MSc thesis project was to investigate on the cellular mode of action of several inhibitor targeting a wide range of histone lysine methyltransferases and lysine demethylases.
This was performed by combining a new mass spectrometry-based technology as well as phenotypic assays.
Our strategy was to analyse the effects of a panel of inhibitors on the abundance of more than 100 histone PTMs by histone epi-proteomics in HeLa cells and determine the effects in respect of selected glioma cell lines by a flow-cytometry validation assay.

This thesis is performed under the joint supervision of Dr. Tobias Weiss (laboratory of Prof. Michael Weller, Department of Neurology at the University Hospital Zurich) and Dr. Christian Feller (laboratory of Prof. Ruedi Aebersold, Department of Biology, ETH Zurich).

Materials

Cell culture

HeLa Kyoto cells
Adherent glioma cell lines (A172, D247, LN18, LN229, LN308, LN319, LN428, T98G, U87)
DMEM medium *(Invitrogen)*
10% fetal bovine serum *(Gibco Life Technologies)*
2mmol/L L-glutamine *(Gibco Life Technologies)*
Penicillin-streptomycin *(Sigma)*

Suspension cell lines (S24, T325, ZH161, ZH305, ZH562)
Neurobasal medium *(Invitrogen)*
2mmol/L L-glutamine *(Gibco Life Technologies)*
2% B-27 *(Gibco Life Technologies)*
10 ng/mL epidermal growth factor (EGF) *(Pepro Tech London)*
Fibroblast growth factor + Penicillin-Streptomycin *(Pepro Tech London)*

Inhibitor treatments

The inhibitors used for the experiments are listed in Table S1
DMSO *(Sigma)*
DPBS *(Gibco Life Technologies)*
TrypLE Express *(Gibco Life Technologies)*

Histone sample preparation for mass spectrometer analysis

Acid extraction

0.2 M H_2SO_4
0.2% HCl in acetone (at -20°C)
Neutralization Buffer (NB): 1 M Tris-HCl pH 8, 400 mM NaCl, 4 mM EDTA, add freshly before use: 2 mM DTT
Resin Equilibration Buffer (REB): 50 mM Tris-HCl pH 8.0, 2mM EDTA, 200mM NaCl
Washing Buffer (WB): 50 mM Tris-HCl pH 8.0, 2mM EDTA, 500mM NaCl

Elution Buffer (EB): 50 mM Tris-HCl pH 8.0, 2mM EDTA, 2 M NaCl
Sulfopropyl-Sepherose beads *(Sigma)*
Micro Bio-Spin Chromatography Columns *(Bio-Rad)*
MS-grade water *(Fisher Scientific)*
Tricholoroacetic acid *(Sigma)*
pH paper

BCA assay

Pierce BCA Protein Assay Kit *(Thermo Scientific)*

In-solution histone protein level D3AA derivatization, tryptic digest & peptide-level derivatization

100 mM ambic
D6-deuterated acetic anhydrid *(Sigma)*
1 M ammonium bicarbonate (ambic) in MS-grade water
Trypsin *(Promega)*, prepared as 50 ng/µL stock in ambic

Desalting

100% Methanol
80% ACN + 0.1% TFA
50% ACN + 0.25% TFA
60% ACN + 0.1% TFA
0.1% TFA
10% TFA
0.1% FA
StageTip columns: 1 layer of hypercarbon *(Empore Extraction Disk with Activated Carbon)* followed by 2 layers of C18 resin *(Empore C18)* manually prepared in p200 pipette tips

Histone mass spectrometry acquisition

iRT peptides *(Biognosys)* in 0.1% TFA
ReproSil-Pur C18-AQ, 1.9 µm HPLC column *(Maisch)*
Buffer A (0.1% FA in HPLC-grade water)
Buffer B (0.1% FA in ACN)

Flow Cytometry

12-well plates
96-well FACS plates, U bottom
Zombie NIR dye *(BioLegend)*
PI-staining solution: propidium iodide *(Sigma)*, RNase *(Carl Roth AG)* Triton X-100
FACS-buffer: PBS, 0.5% BSA *(Axonlab)*, 0.02% NaN3, 1 mM EDTA
Annexin V/PI staining solution (in Annexin buffer): Annexin V Pacific Blue *(BioLegend)*, Propidium iodide *(Sigma)*

Annexin buffer (pH 7.4): 10 mM HEPES, 140 mM NaCl,
2.5 mM $CaCl_2$

Methods

Cell culture

HeLa Kyoto cells and adherent glioma cell lines (A172, D247, LN18, LN229, LN308, LN319, LN428, T98G, U87) were cultured in DMEM medium (+10% fetal bovine serum, 2mmol/L L-glutamine, penicillin-streptomycin).
The suspension cell lines (S24, T325, ZH161, ZH305, ZH562) were maintained in Neurobasal medium supplemented with 2mmol/L L-glutamine, 2% B-27, 10 ng/mL epidermal growth factor as well as fibroblast growth factor together with penicillin-streptomycin.

Inhibitor treatment

The seeding density for the treatment of HeLa cells was adjusted according to the treatment time:

- 1 day treatment time -> 40% confluency
- 3 day treatment time -> 10% confluency
- 6 day treatment time -> seeded as a sub-passage of cells that has been harvested after 3 day treatment; 20% confluency

The cells were seeded one day before treatment. 10x compound pre-dilutions were prepared in culture medium and added to the cells. For each compound cells were treated with two different concentrations and in two biological replicates. Triplicates of cells were treated with 0.2% DMSO for each timepoint as a control.
For the harvesting process the medium was aspirated, cells were washed with PBS and 3mL TrypLE Express (3-5 min at 37°C) was added in order to detach the cells. After stopping the reaction by addition of 6mL fresh medium, the cell suspension was transferred into 15 mL falcon tubes. Subsequently, cells were counted via Vi-Cel XR Cell Viability Analyzer *(Beckman Coulter)*, the cell suspension was centrifuged at 1200 rpm for 4 min and the received pellet was resuspended in cold PBS.

Transferred into a 1.5 mL tube, cells were pelleted again (1-3 aliquots per cell pellet) via centrifugation at 3000 rpm, 4°C, for 4 min. The last step included snap-freezing in liquid nitrogen and storage at -80°C until proceeded.

Histone PTM Sample Preparation Protocol

Acid Extraction

First 500 µL 0.2M H_2SO_4 was added to every sample. In case one sample aliquots contained less than 3 million cells, both aliquots from this sample were pooled. Afterwards each suspension were placed in a thermo shaker at 800 rpm, 4°C for 3 hours.

Histone clean-up using Sulfopropyl-Sepharose beads

After clearing (samples spinned down 10-30 min full speed at 4°C) 480 µL of each supernatant (basic proteins are expected to be in solution) were transferred to a new 1.5 mL Eppendorf tube and neutralized by adding 480 µL neutralization buffer.
For the equilibration of the required Sulfopropyl-Sepharose (SP) beads, beads were transferred into 15 mL falcon tubes, centrifuged at 20g for 1 minute, washed once with 10x volume H_2O and three times with 10x volume RB-buffer. After the washing steps, beads were resuspended in 200 µL RB-buffer per sample. 150 µL of bead suspension was added to the neutralized cleared lysate. Subsequently, incubation on spinning wheel for ~30 min was performed. Required columns were washed once with 500 µL RB-buffer, bead/histone solution was added and centrifuged. Columns were washed 3 x with 500 µL washing buffer. For the elution the columns were placed into new 2 mL tubes and eluted twice with 150 µL elution buffer.

TCA precipitation

For TCA precipitation the solution was transferred to 1.5 mL tubes and 100 µL of 25% TCA were added. Precipitate were stored overnight at 4°C.

Acetone washes and Reconstitution

After TCA precipitation, the tubes were centrifuged at 4°C maximum speed for 60 minutes. Afterwards, the supernatant was removed carefully without disturbing the pellet and the precipitates that form along the tube wall. The next 3 steps included the washing with 900 µL ice-cold acetone + HCl (0.2%) respectively 900 µL ice-cold acetone only. After the washing steps, the supernatant was removed to let the pellet dry.
For the reconstitution the histone pellet was dissolved in 40 µL mass spec grade water.

BCA, Derivatization and Trypsin digest

For the quantification of the protein amount used for Derivatization and in-solution digestion, Pierce™ BCA Protein Assay was applied [BCA assay, Derivatization, Tryptic digest performed by Christian Feller].

Desalting

Before the desalting ptocess, stage tips needed to be prepared as following:

1.) + 70 µL 100% Methanol -> conditioning
2.) + 70 µL 80% ACN + 0.1% TFA -> wetting
3.) + 140 µL 0.1% TFA -> equilibration

Samples were loaded to the column, washed with 140 µL 0.1% TFA, 70 µL 0.1 TFA and eluted twice with 1x 80 µL 50% ACN + 0.25% TFA and 1x 50 µL 60% ACN + 0.1% FA. The eluate was vacuum concentrated until 1-2 µL volume remained.
For MS acquisition peptides were resuspended in 20 µL of 1:25 iRT-peptide in 0.1% TFA. Afterwards 2 µL of the peptide solution were mixed with 18 µL of iRT-solution, centrifuged at top speed for 30 minutes and transferred to MS-vials.

Mass spectrometry measurement and Data analysis

The samples were then measured on a Thermo Q-Exactive HF mass spectrometer *(Thermo Fisher Scientific)* using a DIA-PRM mode. For the dataset analysis Skyline, Excel and RStudio as well as Adobe Illustrator, for graphical illustrations, were used. Therefore, the received output file was imported into Skyline-Daily software where the automated peak selection, which was performed on the basis of the retention time and the MS2 spectra, was manually verified. The abundancy of each peptide of interest were then quantified as the area under the curve of the related MS1 chromatogram peak. Afterwards an export file was created and further analysis were performed using the RStudio statistical computing environment.
For calculation of fold-changes (FC) for inhibitor-treated cells, the calculated stochiometry value of each peptide was divided by the mean relative abundance of the DMSO-treated cells.
The specificity of each of the inhibitor were calculated as the absolute value of the mean $\log_2$(FC) across the expected target sites or expected target sites plus related motifs (combinatorial), divided by the mean $\log_2$(FC) of all measured histone PTMs.

Flow Cytometry

The day before treatment the cells were counted via Vi-Cel XR Cell Viability Analyzer *(Beckman Coulter)* and seeded in 1 mL of respective medium into 12-well plates. The seeding density was estimated based on a desired confluency of 80% after 6 days of growth. For each cell line, cells were seeded in triplicates.
The following day 1 mL of 2x compound dilution, that was prepared in respective medium and added to each well containing the target cells. For a negative control, cells were treated with 10 µM staurosporine 3 hours before starting the harvesting. For the FACS analysis the treated cells needed to be transferred into a 96-well plate (U-bottom) which required a washing step with PBS and subsequent detachment by adding 150 µL accutase to each well. As soon as the cells were transferred, they were prepared for the staining procedure by washing with PBS, followed by centrifugation for 5 minutes at 1200 rpm and removal of medium.

Cell cycle FACS

Regarding the life-dead staining with Zombie-NIR, pelleted cells were dissolved and incubated for 30 minutes in 50 µL of pre-diluted Zombie-NIR dilution (1:200 in PBS). After the incubation time, the plate was centrifuged (5min, 1200 rpm), cells were washed with PBS and resuspended in 180 µL cold ethanol. After storage overnight at 4°C permeabilised cells were pelleted and washed with PBS in order to proceed with resuspension in 140 µL PI master solution (50 µg/mL PI, 100 µg/mL RNase and 0.1% Triton). Incubation duration was 30 minutes at 4°C. It´s important to ensure light protection. Afterwards cells were washed and resuspended in 200 µL FACS buffer (0.5% BSA, 0.02% NaN_3, 1 mM EDTA in PBS)

Annexin V/PI FACS

Cells were washed once with annexin buffer (10 mM HEPES, 140 mM NaCl, 2.5 mM $CaCl_2$, pH 7.4) after transfer to the 96-well FACS plate. After centrifugation the received cell pellet was resuspended in 50 µL staining buffer (1:10 Annexin V Pacific Blue and 1:10 PI in Annexin buffer). The 30 minute incubation time was followed by a washing step with 50 µL Annexin buffer. Before performing the measurement, cells needed to be resuspended in 200 µL Annexin buffer.

The FACS measurement was accomplished using a BD FACSverse flow cytometry that provided the automated measurement of a FACS plate due to it´s BD FACS Universal Loader. Each well was measured 150 seconds or until a maximum of 20.000 cells.

Results and discussion

Characterization of inhibitors by histone epi-proteomics

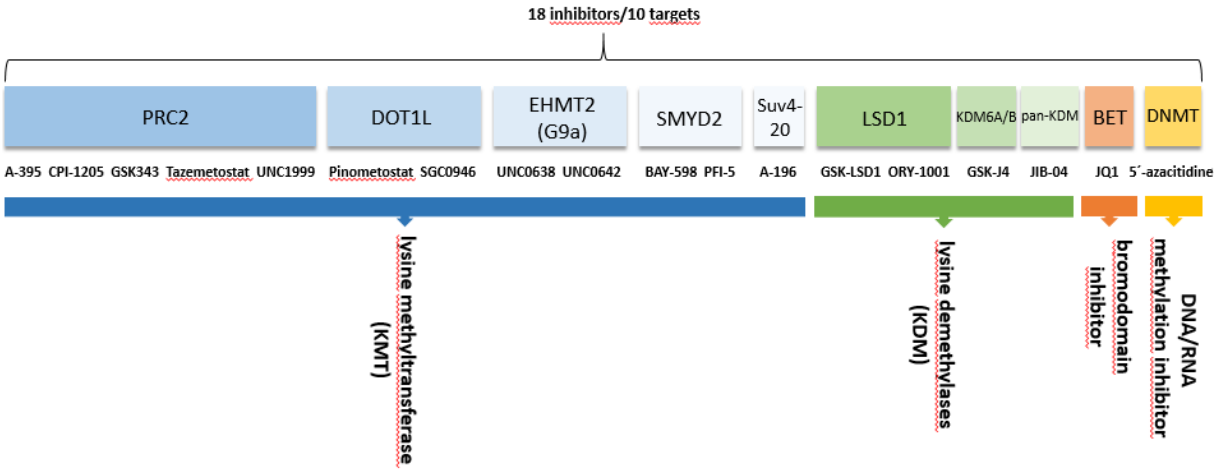

Figure 1: Panel of inhibitors targeting protein-modifying enzymes.

To be able to analyze the cellular mode of action of each inhibitor in detail, we decided to treat the cultured HeLa cells

- using different inhibitors targeting the same protein,
- with two different concentrations *(GSK-J4:* 2 & 10 µM*; 5-azacitidine:* 5 & 25 µM; all other compounds: 1 & 5 µM), and
- measurement at three different timepoints (1, 3, 6 days)

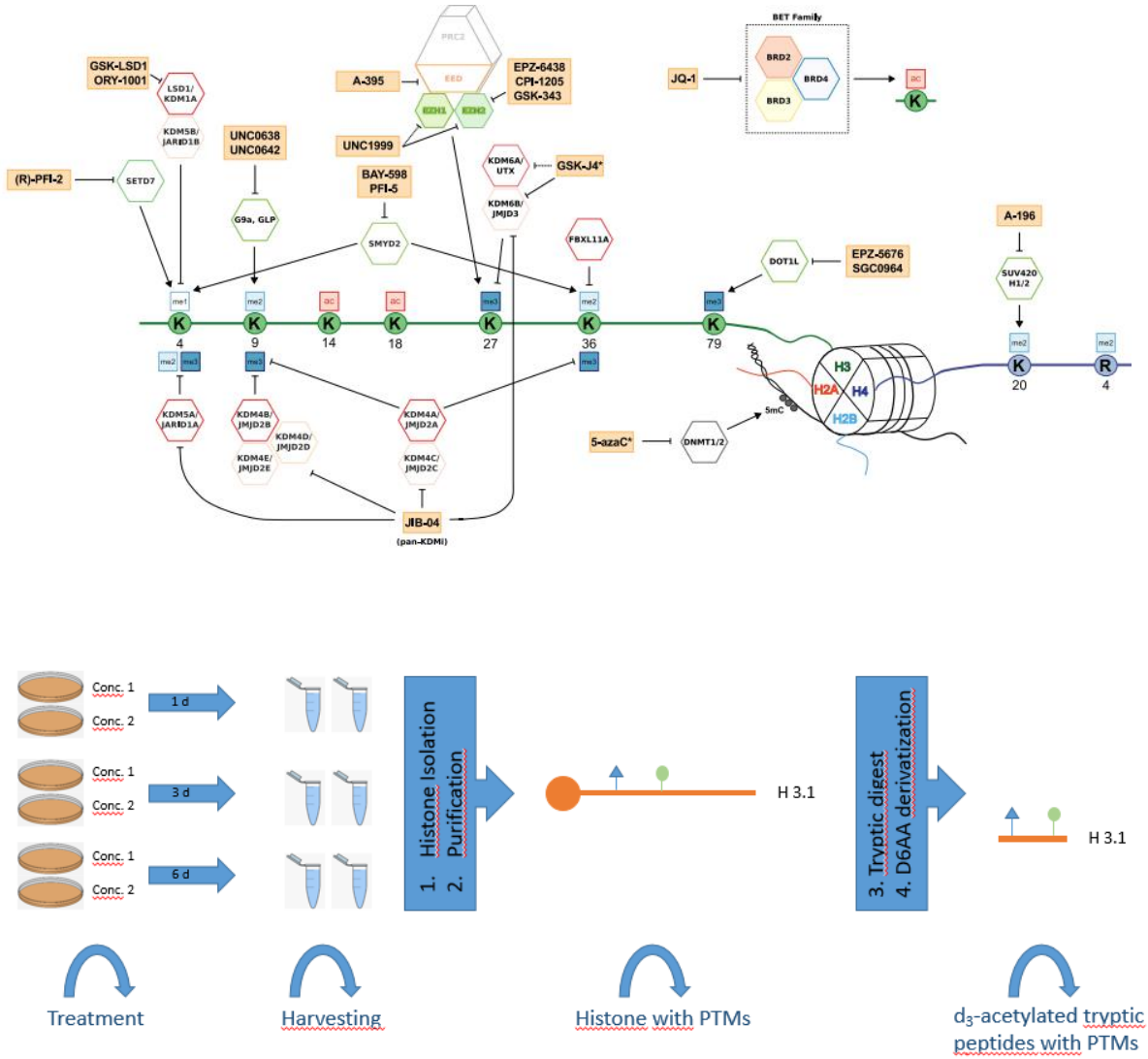

Figure 2: Experimental approach to investigate on the post-translational modification pattern after inhibitor treatement.

After the treatment of HeLa cells with the previous described inhibitors, the histones needed to be extracted and processed until the peptides were received.
Mass spectrometry allowed us to analyse the different post-translational modifications with high confidence.
The quantification of abundancy of the modifications was accomplished relative to DMSO treated cells.
In respect of the used compounds, besides the inhibitors targeting a broad range of KMT and KDM, the experiment also includes the DNA/RNA methylation inhibitor 5-

azacitidine and the pan-KDM inhibitor JIB-04. 5-azacitidine is already approved from the FDA and several other compounds such as Tazemetostat, Pinometostat/EPZ-5676, ORY-1001 and CPI-1205 are currently in clinical trials.

Application of a new mass spectrometry-based approach for the investigation on an inhibitor-induced modification pattern

One of the main aspect of the MSc thesis project was to investigate on the cellular mode of action of inhibitor targeting epigenetic proteins using a new histone epi-proteomics technology *(Feller et al., 2015; Schworer et al., 2016, manuscript in preparation).*

In order to prove the reliability of the method, CoVs were calculated for each measured peptide across all DMSO controls.

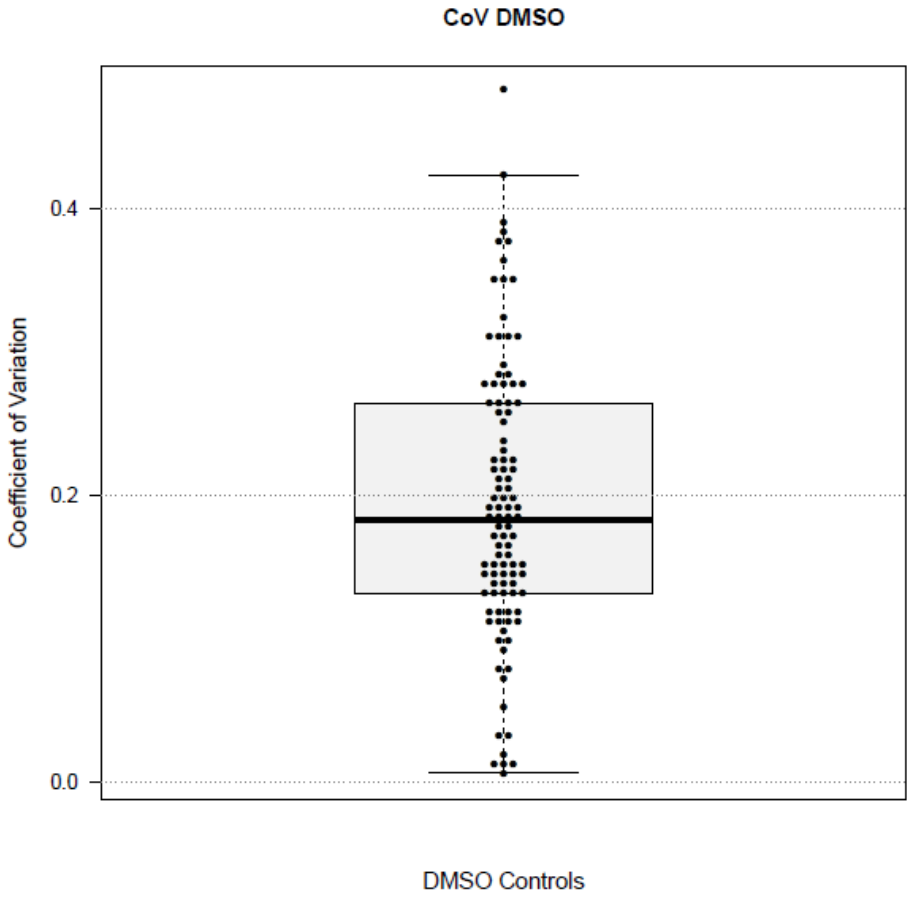

Figure 3: Coefficient of Variance determined for the reliability of the mass spectrometry-based approach.

As shown in Figure 3 the median CoV is below 20%. Except of two peptides the CoV does not exceed the 40% mark which is a tolerable variation.

For an general overview of the overall changes of the histone PTM motifs after inhibitor treatment, the received data were averaged across all time points and both concentrations.

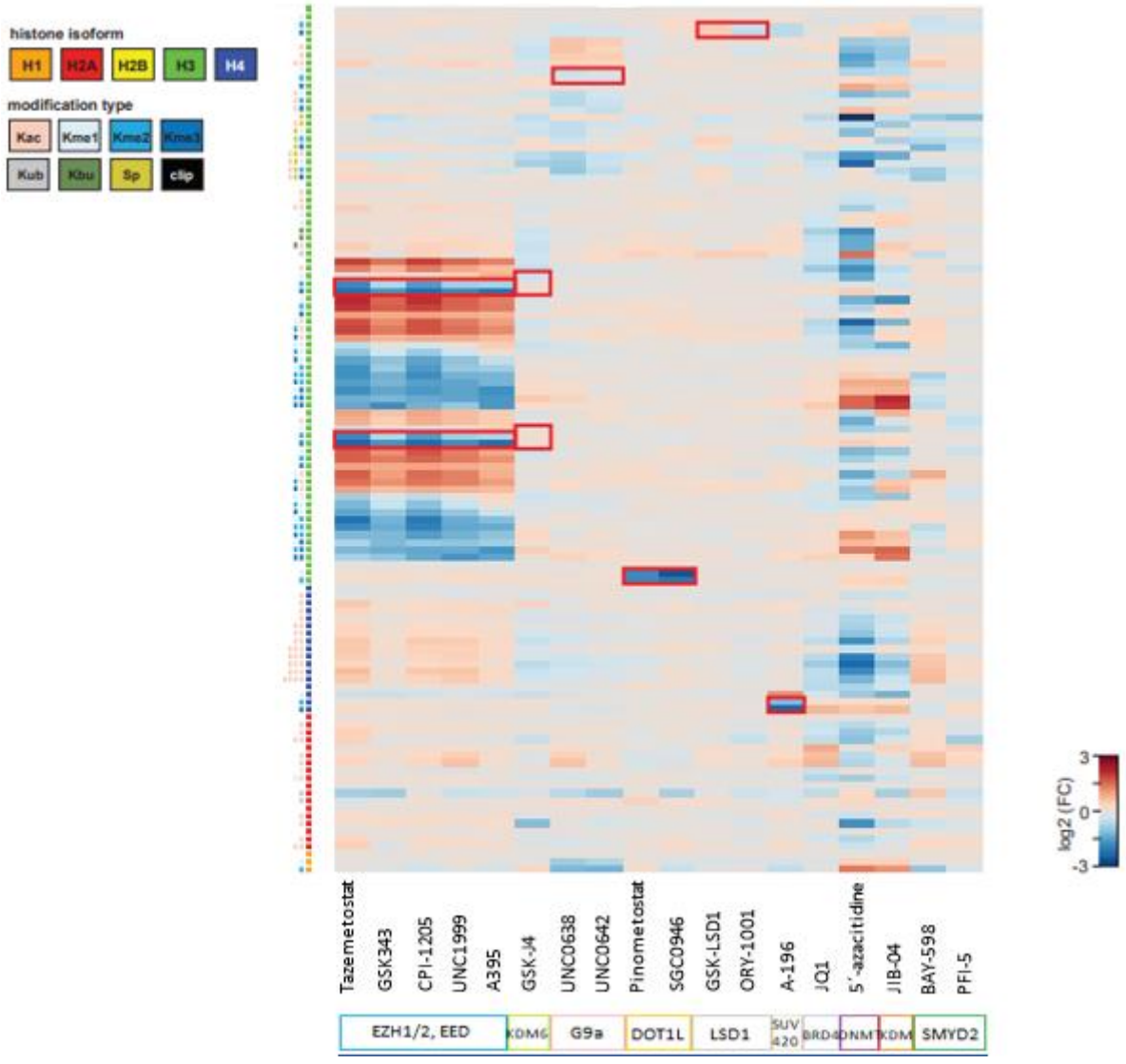

Figure 4: Heatmap displaying the effects on 114 histone motifs after inhibitor treatment. Quantification by the log_2 fold-change (FC) relative to DMSO control.

Due to the 5´-azacitidine induced inhibition of DNA methylation a broad effect regarding changes in peptide abundancies was expected. Having a look at the heatmap (Fig.4), changes in more than half of the motifs can be observed.
Same suggestion held true in respect of the compound JIB-04 whose target are pan-KDM.
On the other hand there are compounds that show a very specific response pattern such as the DOT1L inhibitors Pinometostat and SGC0946: both induced a significant decrease in their target modifications (H3K79me1/2), which exhibits their specificity.
Also beyond debate is the specific effect of the Suv4-20 inhibitor A-196 that shows a strong decrease in H4K20me2/3, therefore confirming the suggested primary target.
Having the hypothesis of the histone code in mind, the PRC2 inhibitors revealing an interesting response pattern: besides the decrease in their primary targets H3K27me2/3, there are several changes in other modifications. A reduction in combinatorial motifs consisting of different methylation states of H3K27 and H3K36 was observed. Furthermore modifications that are associated with gene activation like the monomethylation of H3K36 in combination with acetylation of H3K27 are increased.
Regarding the other investigated compounds (GSK-J4, UNC0638, UNC0642, PFI-5, BAY-598, JQ1) there are surprisingly weak or even no effects at their primary target sites.
Concerning the both LSD1 inhibitor the suggestion would be an increase in methylation of lysine 4 on histone 3, but the data provide just a slight increase upon treatment with GSK-LSD1 and actually a decrease when cells were treated with ORY-1001.

PRC2 Inhibitors

The histone methyltransferases EZH2/EZH1 (enhancer of zeste homologue-subunits) are embedded in the PRC2 complex and responsible for di- and tri-methylation of lysine 27 on histone 3 (H3K27). Due to the overexpression of EZH1/2 in several solid tumors the PRC2 complex provides a promising target for treatment strategies.

The PRC2 complex consists of four components: EED, EZH1/2, SUZ12 and RbAp46/48 that are required for it´s enzymatic activity.

PRC2 is important for transcriptional repression of many genes including critical regulators in development and differentiation. Therefore PRC2 proteins are also essential for normal embryonic development [14].

EZH2 is widely implicated in cancer progression, largely due to it´s prevalent overexpression that is associated with a significant increase in H3K27 methylation, disease stage, and poor prognosis [15, 16, 17].

Due to the fact that EZH1 and EZH2 targeting the same genes they are expected to affect the same silencing pathway.
Such as H3K9me3 is a benchmark of transcriptionally silenced genes, so is H3K27me3 [18, 19].

Except for A-395 which inhibit the reader protein responsible for EZH2 substrate recognition [20] and GSK343 that inhibits EZH2/EZH1, the tested PRC2-inhibitors are very similar: they are all SAM-competitive inhibitors and effective in a low nano-molar range.

Similar to the previous described compounds, GSK43 is a small molecule inhibitor selective for EZH2 and leads to a downregulation of H3K27me3 in HCC1806 breast cancer cells. A growth inhibiting effect of GSK343 was observed in several breast and prostate cancer cell lines [21].

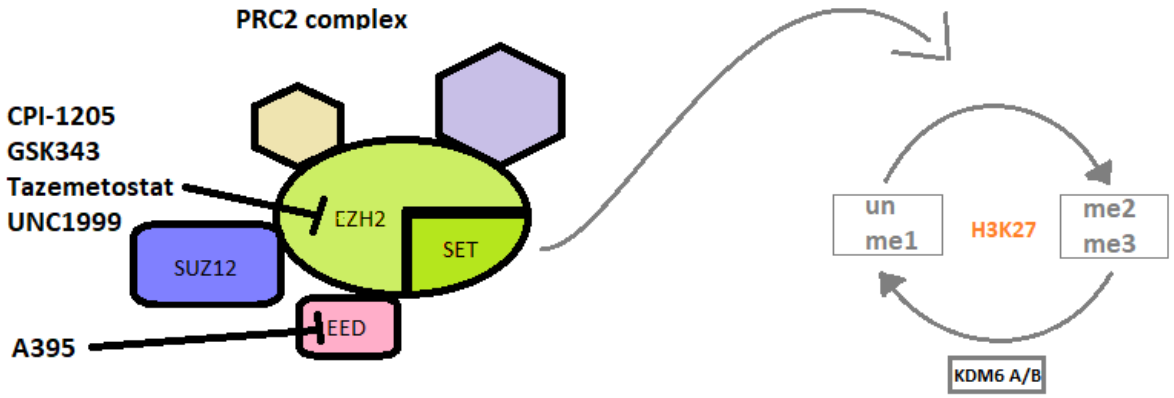

Figure 5: Inhibitors targeting the PRC2 complex whose methyltransferase subunit EZH2 is responsible for di- and trimethylation of H3K27. Demethylases of the KDM6 family working as an antagonist.

As previously described, the primary targets of the EZH1/2 & EED inhibitors H3K27me2/3 are confirmed through the observed decrease of methylation (Fig. 6). We observed that the di- and tri-methylation states of histone 3 lysine 27 (H3K27) decreased upon the treatment with 1µM and even stronger when treated with 5µM.

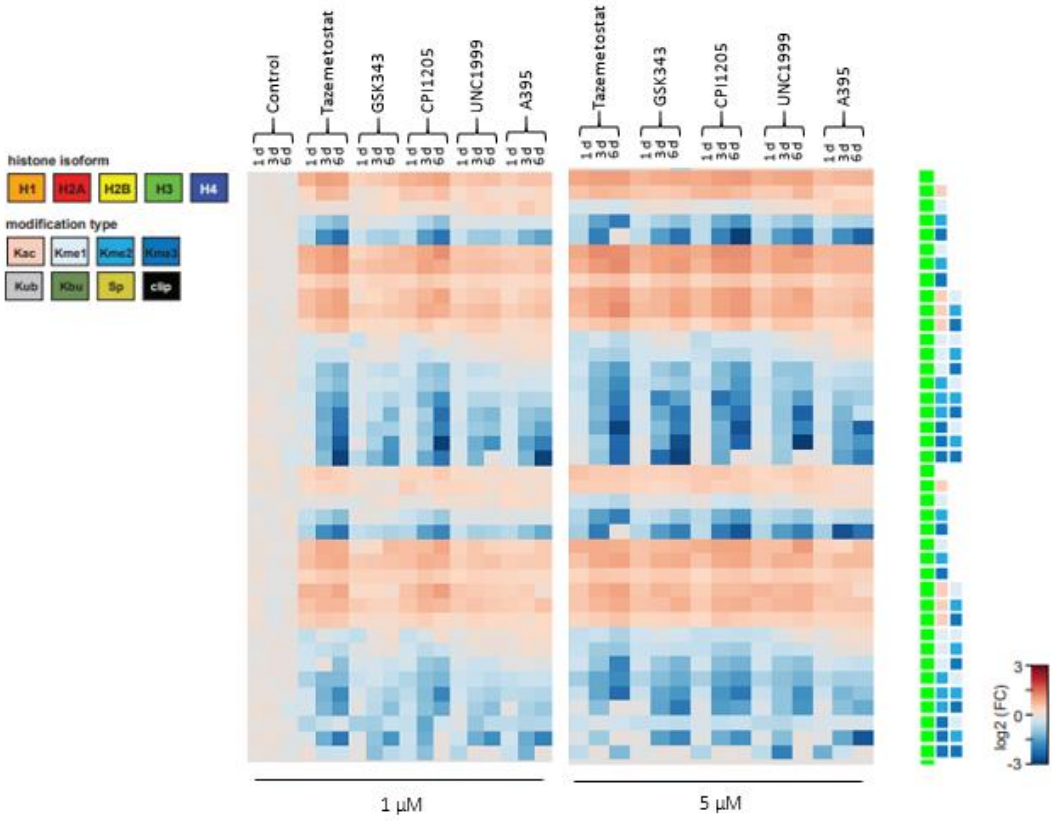

Figure 6: Broad response pattern in HeLa cells after inhibition of EZH2/EED of the PRC2-complex.

The opposite observation holds true while looking at the abundance of the monomethylated lysine when treated with A-395: a significant increase was observed. The other four compounds did not have a clear effect in this regard.

The reduction of abundance is even stronger for H3K27me3 than for H3K27me2. This observation is valid for each of the investigated inhibitors (Fig. 6).

The previous described effect was observed upon EED and EZH2-inhibition, which indicates that the inhibitors cellular mode of action is either because of a reduced binding-affinity of PRC2 to the histone or due to an inhibition of it´s function to promote methyltransferases. The latter explanation can be confirmed according to the findings of Simon and Kingston that EED support the enzymatic activity of the methyltransferase subunit EZH2 [22].

An increase in unmethylated H3K27 was observed in all cases, which lead to the assumption that the inhibition of PRC2 engender a complete demethylation at this side.

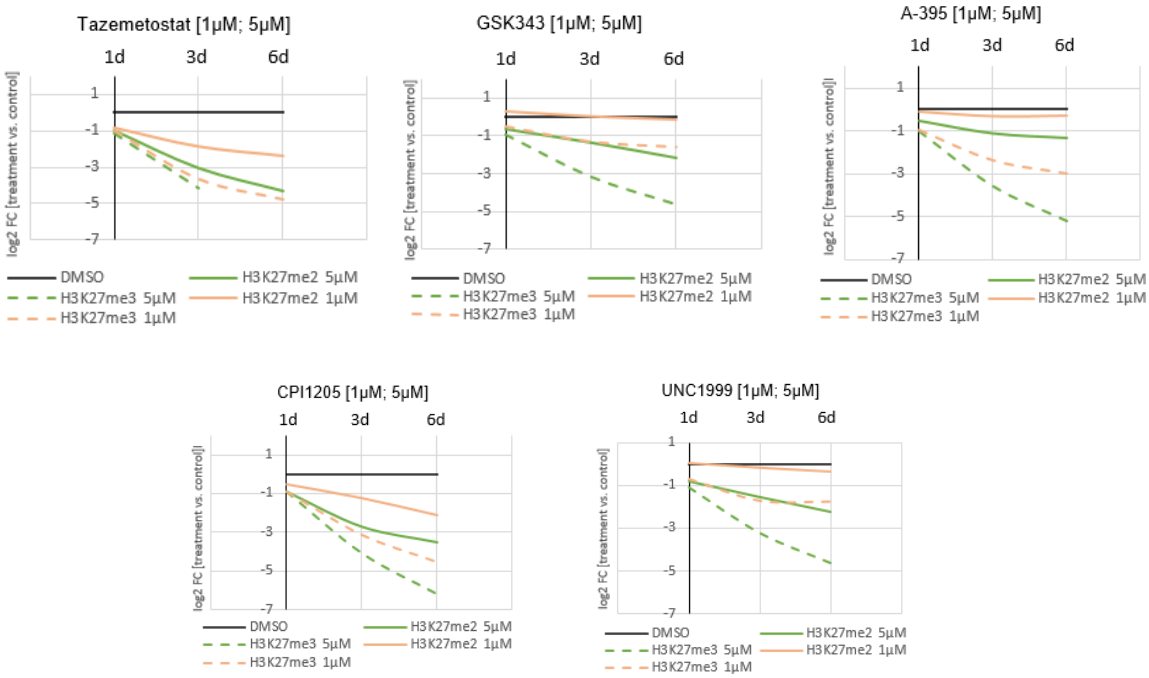

Figure 7: Inhibitor induced effects on the di- and trimethylation of H3K27 with either 1 µM or 5 µM over a time-course of 6 days.

Especially for A-395 there is a strong decrease regarding the trimethylation of histone 3 lysine 27 in both concentrations (Fig. 7).

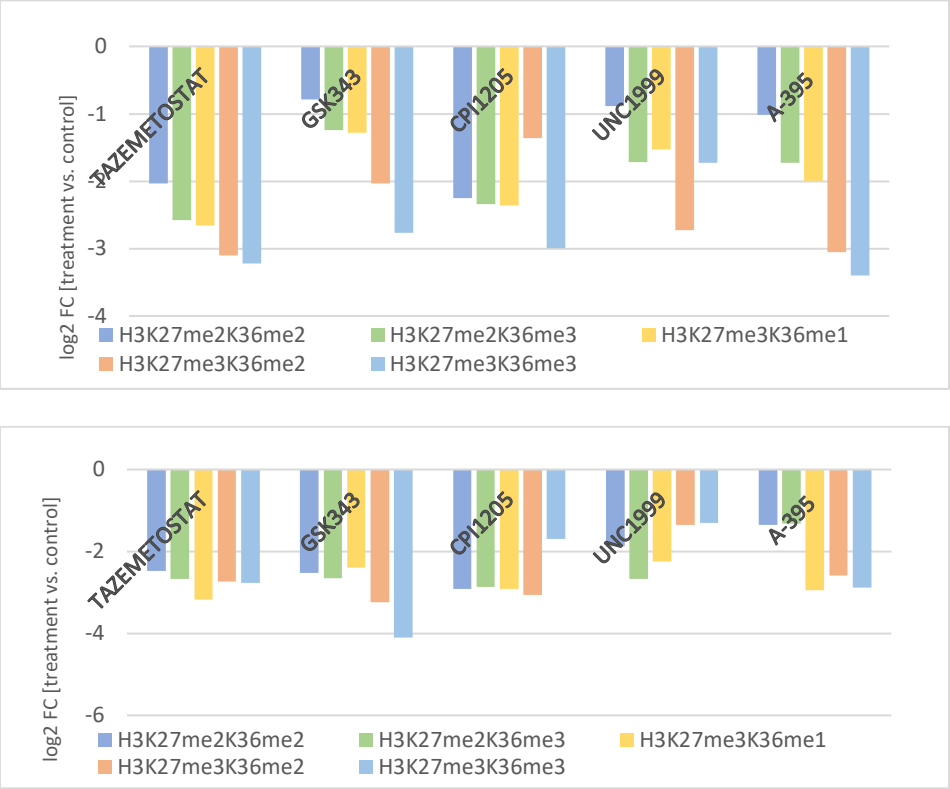

Figure 8: Upper picture 1 µM. Lower picture 5 µM.

Returning to the histone code hypothesis, methylation on H3K27 co-occur with methylation on lysine 36 on histone 3 [4]. This supposition is due to the fact that lysine 27 is in close proximity of lysine 36, whose methylation is associated with actively transcribed genes.

Beside UNC1999, for each of the inhibitor the strongest reduction occur when both lysines are trimethylated (H3K27me3K36me3). The weakest but still significant decrease was observed when lysine 27 as well as lysine 36 are dimethylated (Fig. 8).

However, the methylation state of lysine 36 on histone 3 (H3K36) does not seem to play a role when H3K27 is acetylated: an increase in abundance was observed which supports the suggestion that this may be a compensatory effect initiated through the loss of H3K27 methylation (Fig. 6).

Underlining the importancy of such an effect, Huang et al. observed that different levels in the gain of acetylation of H3K27 upon treatment with Tazemetostat in different cancer cell lines, correlates with the resistance of EZH2 inhibition [23].

Whereas there is a strong reduction in methylation when lysine 27 is di- or trimethylated and lysine 36 is either mono-, di- or trimethylated.

An interesting observation, that confirm the observation of a previous experiment (Daniel Schirmacher thesis), is that the monomethylated H3K27 is also reduced when lysine 36 is trimethylated (Fig. 9).

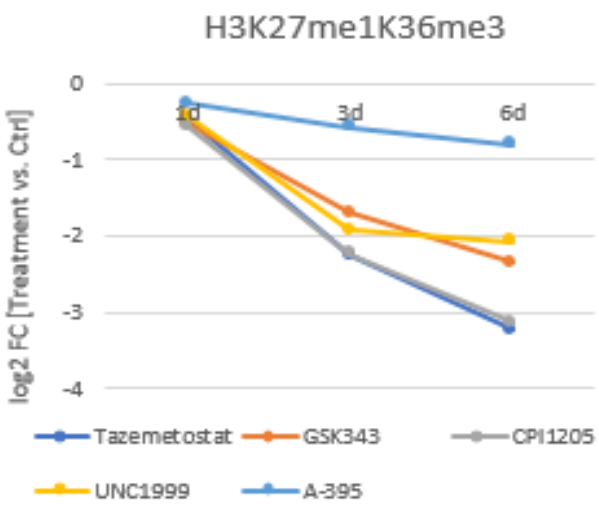

These observations lead to the assumption that there is indeed a cross-talk in respect to different modification states.

Figure 9: Effects of compound treatment inhibiting the PRC2-complex (5 µM). Combinatorial motif H3K27me1K36me3 showed a decrease in both concentrations.

Most potent PRC2 inhibitor

Having a look at the Figure 10, the barplots that display the changes in histone motifs, almost show the same pattern. Red bars indicate the main targets, the blue ones show the related targets and the grey bars are the suggested off targets. In respect of the potency of the EZH2 inhibitor Tazemetostat and CPI1205 show the strongest decrease in several methylation states. Tazemetostat actually has such a strong effect of some motifs that there is not any remaining detectable signal left.

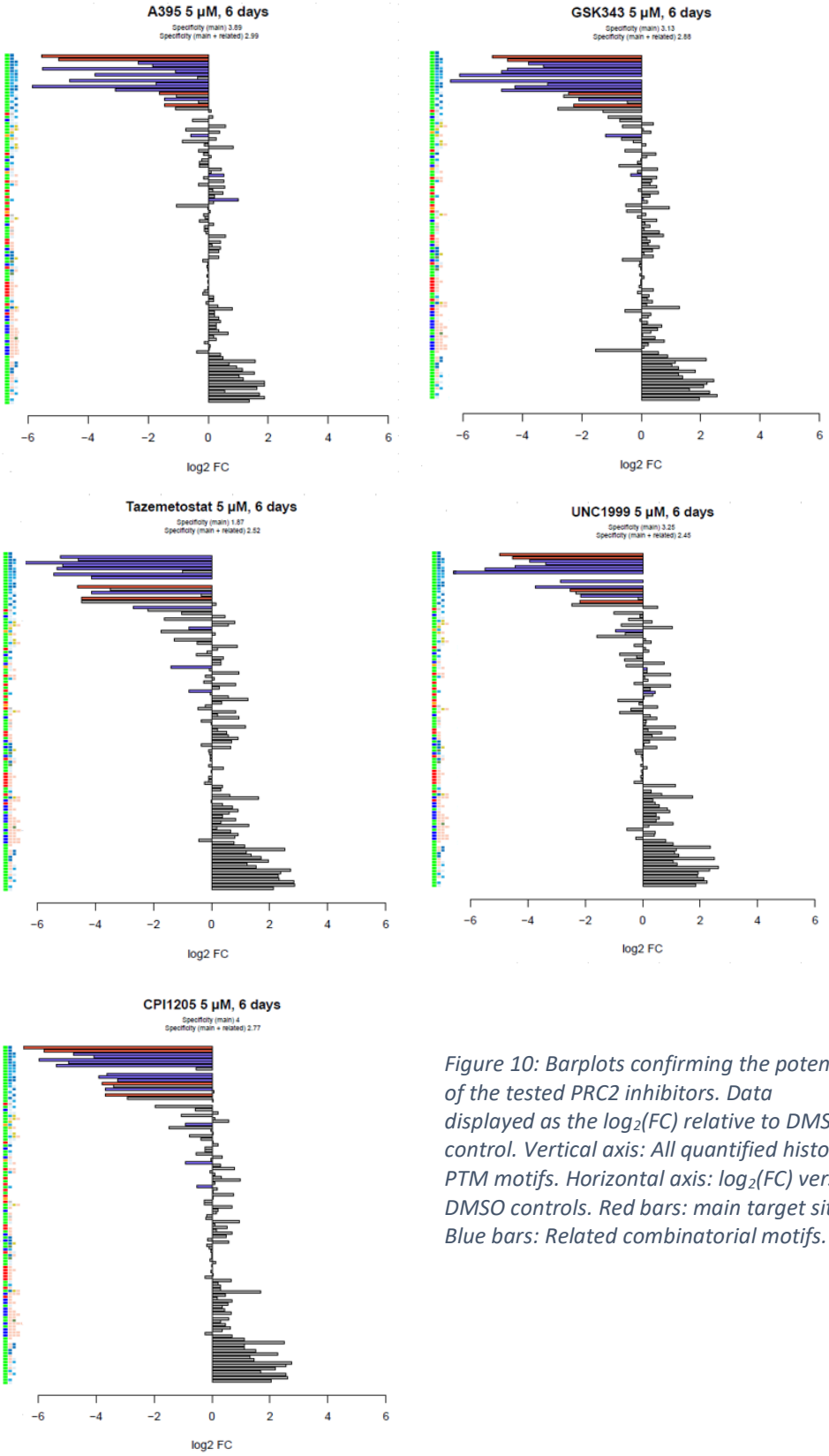

Figure 10: Barplots confirming the potency of the tested PRC2 inhibitors. Data displayed as the log_2(FC) relative to DMSO control. Vertical axis: All quantified histone PTM motifs. Horizontal axis: log_2(FC) versus DMSO controls. Red bars: main target sites; Blue bars: Related combinatorial motifs.

G9a inhibitor

In 2002, Tachibana and his colleagues revealed the importance of balanced G9a level in their study `G9a histone methyltransferase plays a dominant role in euchromatic histone H3 lysine 9 methylation and is essential for early embryogenesis`. According to their results lower level are associated with developmental defects as well as lethality in G9a-deficient mouse embryos [24].

An overexpression of G9a, on the other hand, leads to the development of hepatocellular carcinoma, B cell acute lymphoblastic leukemia and non small-cell lung cancer cells [23, 25, 26].
Based on the increased G9a-level an increased dimethylation of lysine 9 on histone 3 around the promoter of the gene CASP1 could be observed. As a result this gene becomes silenced and promotes, as a consequence, tumor cell growth and invasion [26].

Needless to say that finding methods to inhibit G9a activity with small-molecule inhibitors are of large interest, having in mind that non small-cell lung cancer is one of the leading causes of cancer-related death worldwide [26].

G9a (EHMT2) and GLP (G9a-like-protein, EHMT1) reported primary targets are the mono- and dimethylation of H3K9. Another reported target is H4.1K26 and H3K27 methylation [27, 28, 29].

Regarding a strategy to inhibit the methylation activity of G9a there are two possibilities: either through an inhibitor that act as a competitor to the peptide substrate or via the co-substrate SAM (S-Adenosyl methionine), which act as the methyl group donor.

As the first specific inhibitor of G9a and GLP UNC0638 was developed in 2011. It acts as a competitor for the peptide substrate.

Vedadi et al. demonstrated that in the treatment with UNC0638 in MDA-MB-231 cells the dimethylation of lysine 9 on histone 3 decreased. On the other hand, the data interestingly showed an increase in the acetylation of lysine 14 on histone 3 [30].

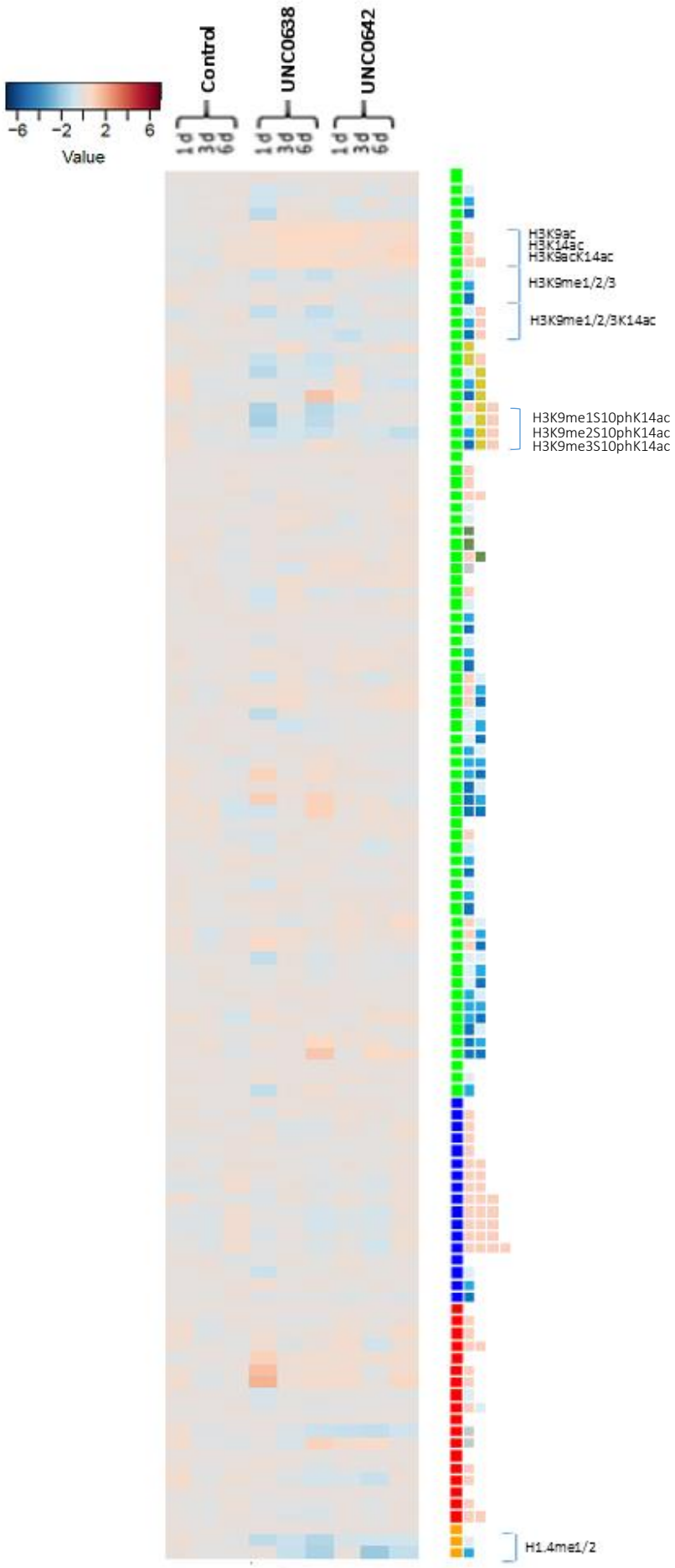
Control
UNC0638
UNC0642
1d
3d
9d
−6
−2
2
6
Value
H3K9ac
H3K14ac
H3K9acK14ac
H3K9me1/2/3
H3K9me1/2/3K14ac
H3K9me1S10phK14ac
H3K9me2S10phK14ac
H3K9me3S10phK14ac
H1.4me1/2

Figure 11: Overall weak response pattern after treatment with G9a-inhibitors UNC0638 and UNC0642.

To improve the pharmacokinetic properties of the inhibitor, UNC0642 was created based on the structure of UNC0638 [31].
This new G9a/GLP-inhibitor showed therapeutic effects in a Prader-Willi syndrome mouse model through the reduction of H3K9me2 at the imprinted regions that are responsible for Prader-Willi syndrome. This led to a better survival [32].

The inhibition is expected to induce a decrease in methylation of H3K9me1 as well as H3K9me2.

The comparison of the effect on the mono- and dimethylation of lysine 9 on histone 3 is shown in Figure 12.

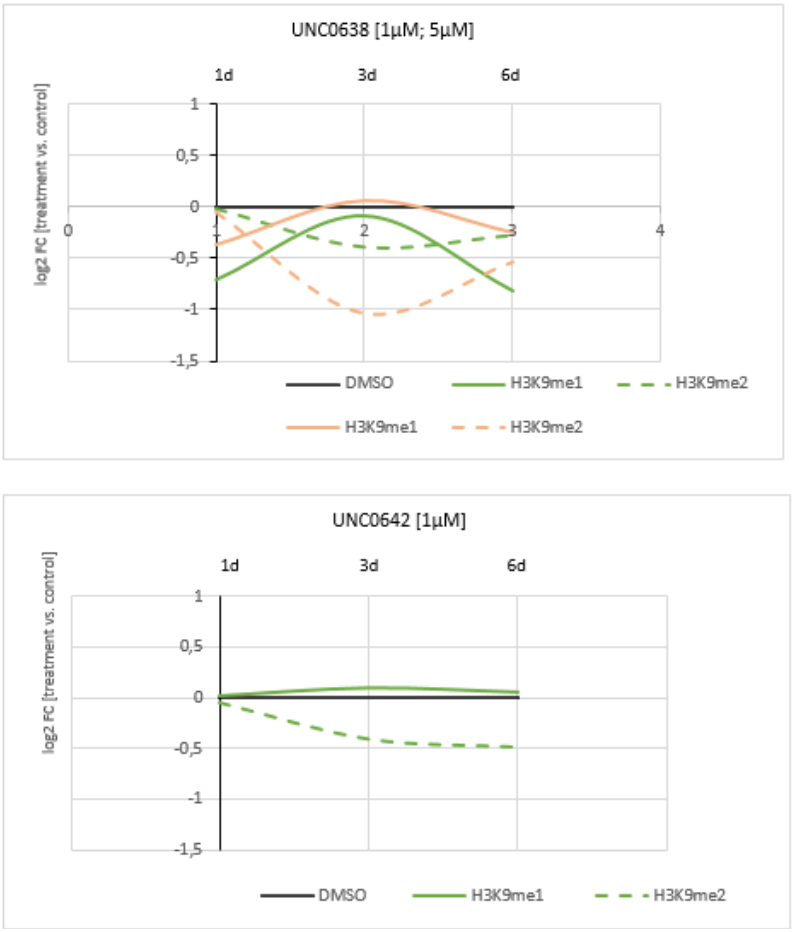

Figure 12: Effects of the G9a inhibitor UNC0638 & UNC0642 on the mono- and dimethylation of H3K9.

When cells were treated with UNC0638 the monomethylation of H3K9 surprisingly shows an increase of abundance after 3 day treatment. However, a subsequent decrease, striving to the baseline, was observed after 6 days of treatment. Therefore, a time- and concentration-dependiency could not be determined. The same holds true for treatment with UNC0642.

Regarding the second known primary target H3K9me2 the inhibitor treatment elicit approximately the same response for both inhibitors. There is a decrease in abundance of dimethylation of about 50% compared to the DMSO control.

All in all the effect of both inhibitor were only moderate.

Coming back to the suggested histone code hypothesis acetylation seems to play a role in decreased methylation levels of H3K9.

As shown in Figure 13 the dimethylation of lysine 9 is even more decreased when lysine 14, which is in close proximity, is acetylated. For both inhibitor the decrease were even more pronounced at later timepoints (6d treatement). Furthermore, the strongest decrease in abundance showed up for motifs with H3S10-phosphorylated peptides (Fig. 11). That indicates a potential cytotoxicity due to the findings of Sawicka et al. who revealed the importance of phosphorylation for cell cycle progression [45].

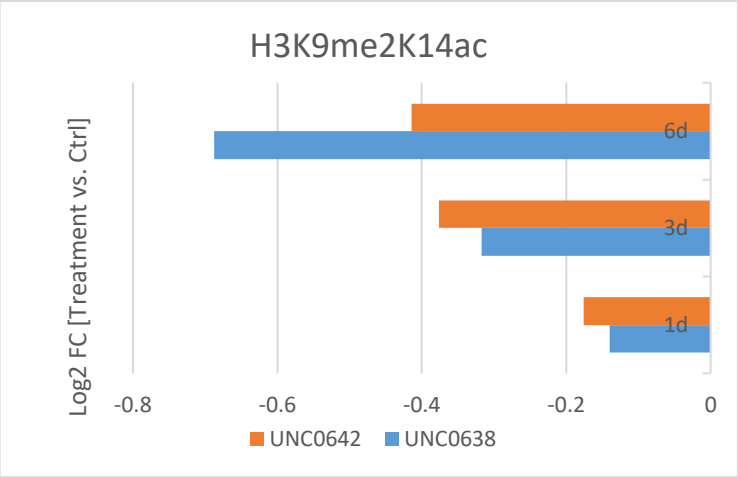

Figure 13: When H3K14 is acetylated, the decrease of demethylation on H3K9 is even stronger which support the hypothesis of a potential cross-talk.

In 2004, Schotta et al. showed up with their investigation on a potential cross-talk between H3K9 and H4K20 methylation [33]. However, our data, in line with the results of Vedadi et al., can not confirm such cross-talk. Under all tested conditions there was

no effect on the di- or trimethylation of H4K20 upon G9a/GLP inhibitor treatment (Fig. 4).

An interesting phenomena showed up when looking at the heatmap in Figure 4: a significant decrease in mono- and dimethylation of histone 1 isoform H1.4 on lysine 25 (H1.4K25me1/2) was observed. This holds true while treatment with both inhibitors, whereas the related unmodified peptide did not show an effect. In 2010, Weiss et al. already showed that methylation of H1.4 is associated with the G9a/GLP-complex in vitro. 5 years later the findings of Hergeth and Schneider et al. confirmed these outcomes (28, 34) . Due to a lack of H1 methylation site-specific modification antibodies, little is known about the function of H1.4 in mammalian cells. Hergeth and Schneider et al. demonstrated a G9a/GLP-dependent methylation of lysine 26 on H1.4 which is associated to serve as a binding platform for heterochromatin protein 1 (HP1). HP1 has transcriptional repressive activity and lead to gene silencing [35].

Compared to the weak effects of UNC0638 and UNC0642 in order of their primary target sites, the strongest responses was induced when H3K9 is mono-, di- or trimethylated while H3S10 is phosphorylated and lysine 14 is acetylated. However, a proof of a cross-talk between the modifications requires further experiments.

In fact, both G9a inhibitors show low overall specificities and potencies.

DOT1L

The reported primary target of the histone demethylase DOT1L is the mono-, di- and trimethylation of H3K79. Methylation of H3K79 is required for several processes like DNA damage response, transcription elongation by RNA polymerase II and cell cycle checkpoint activation [36].

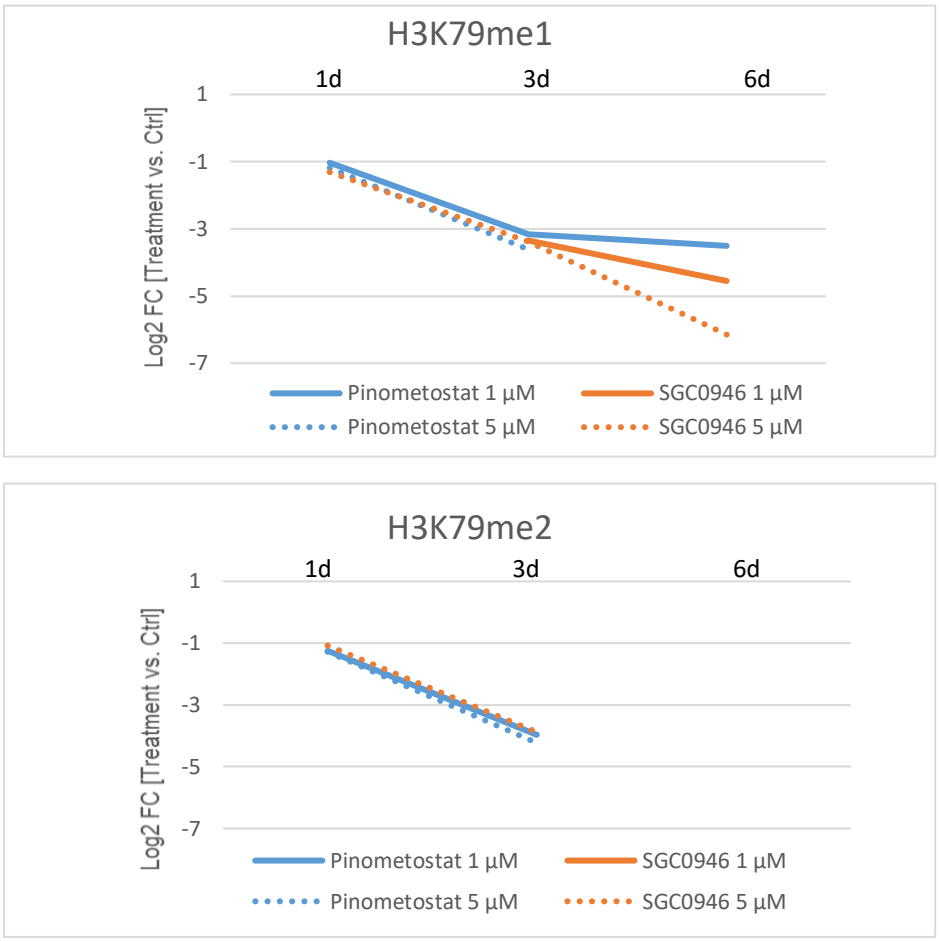

Figure 14: Methylation of H3K79 decreased upon inhibition of histone demethylase DOT1L through Pinometostat and SGC0946.

Treating HeLa cells with either Pinometostat or SGC0946 evoke strong reductions in monomethylation of H3K79 as well as H2K79 dimethylation (Fig. 14). Regarding the dimethylation the decrease was enormously strong after 6 days so that there were no effect detectable.

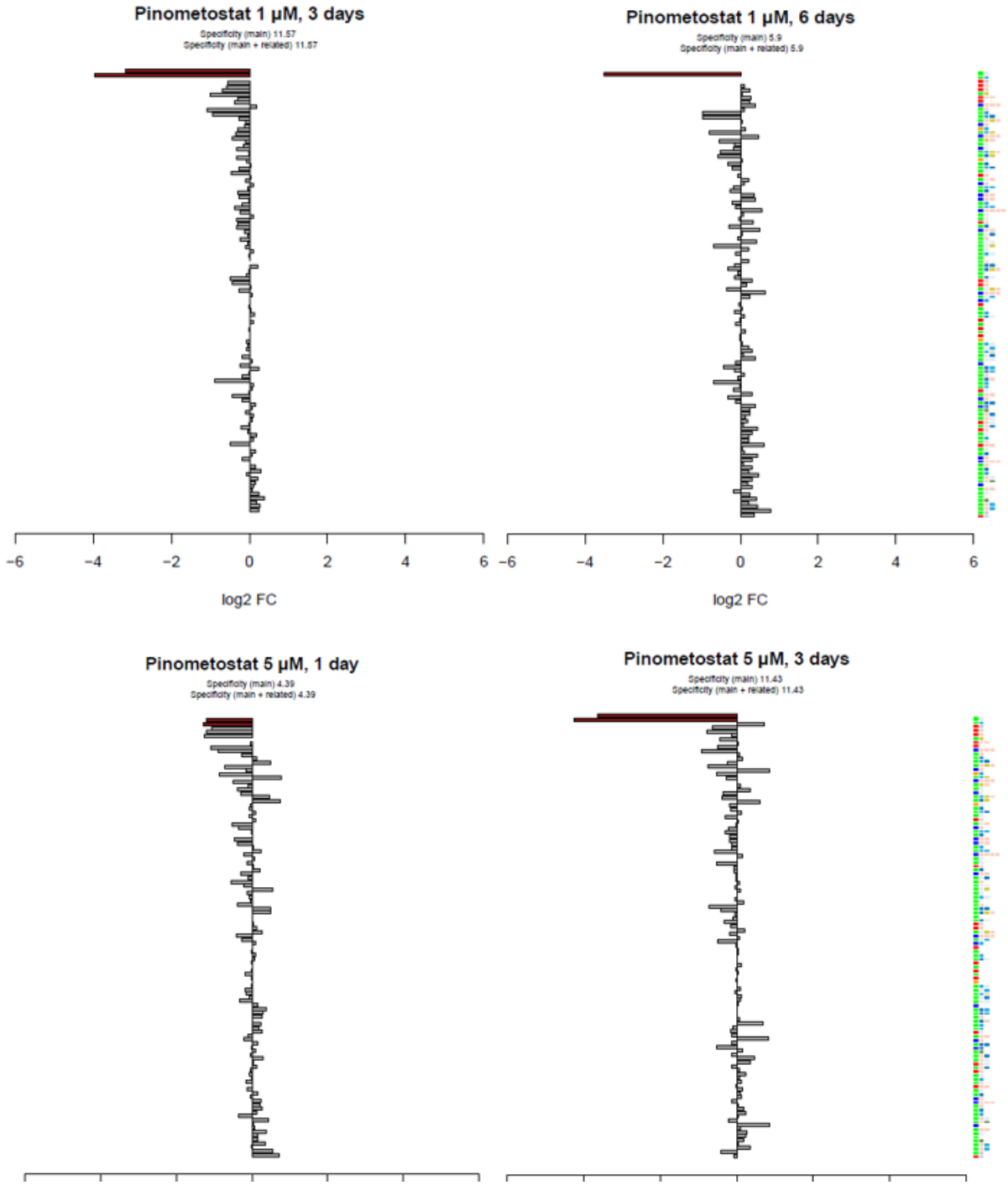

Figure 15: Barplots displaying the high specificity of Pinometostat regarding it´s main target H3K79 (red bars). Vertical axis: All quantified histone PTM motifs. Horizontal axis: log_2(FC) versus DMSO controls.

Having a look at the specificity for the primary target , Pinometostat is highly specific in both concentrations with no significant off-target effects (Fig. 15).

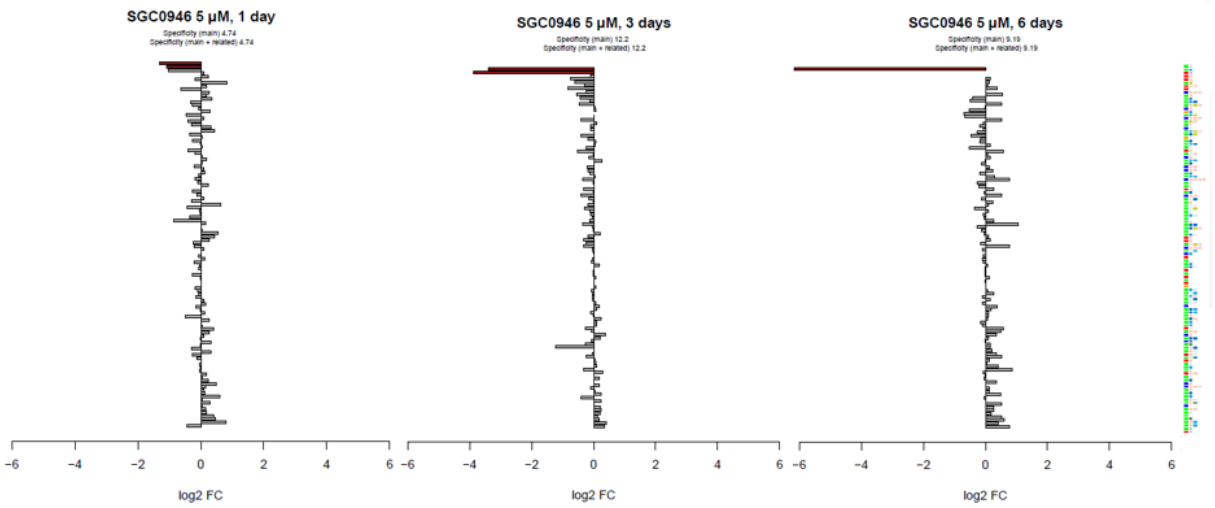

Figure 16: Inhibitor effects of SGC0946 increasing with higher compound concentration.

In contrast to Pinometostat, SGC0946 shows a higher specificity for the primary target when cells were treated with the higher concentration (Fig. 16).

Concluding, the obtained data provide evidence that the tested DOT1L inhibitors causing a strong decrease in their expected main targets, with a high specificity and only little off-target effects.

Selective demethylase inhibitor

GSK-J4

The development of the inhibitor GSK-J1/J4 resulted in the first highly potent and specific compound that targets the H3K27me2/3-demethylases JMJD3/KDM6B and UTX/KDM6A [37].
Demethylation of lysine 27 on histone 3 by JMJD3 is associated with an increased immune response which manifest in inflammation and autoimmune disorders [38]. Therefore, the inhibition of demethylation by GSK-J4 was promising in regard of anti-inflammatory effects. Focusing on the treatment of cells derived from patients who suffer from AML, Li et al. investigated on the potential therapeutic effects of GSK-J4 [39].

In acute myeloid leukemia the mRNA expression of KDM6B is up-regulated and also associated with poor survival. After treatment with GSK-J4 they observed an increase in trimethylation of H3K27 and a decrease in cell proliferation.

Acting as a PRC2 complex antagonist, an increase in methylation after treatment with GSK-J1 as well as with it´s ester derivative GSK-J4 would be expected.

As already observed in the first heatmap (Fig. 4) the responses in order of all investigated motifs are very weak as well as coming along with several off-target effects after treatment with GSK-J4 (Fig. 17).

Figure 18 shows that the increase of dimethylation on H3K27 after 1 day treatment with GSK-J4 is very small and decreases in regard of proceeding treatment time. In contrast, there is an increase, even though it´s just moderate, in trimethylated lysine 27 on histone 3 after treatment of HeLa cells with 10 µM GSK-J4 (Fig. 18).

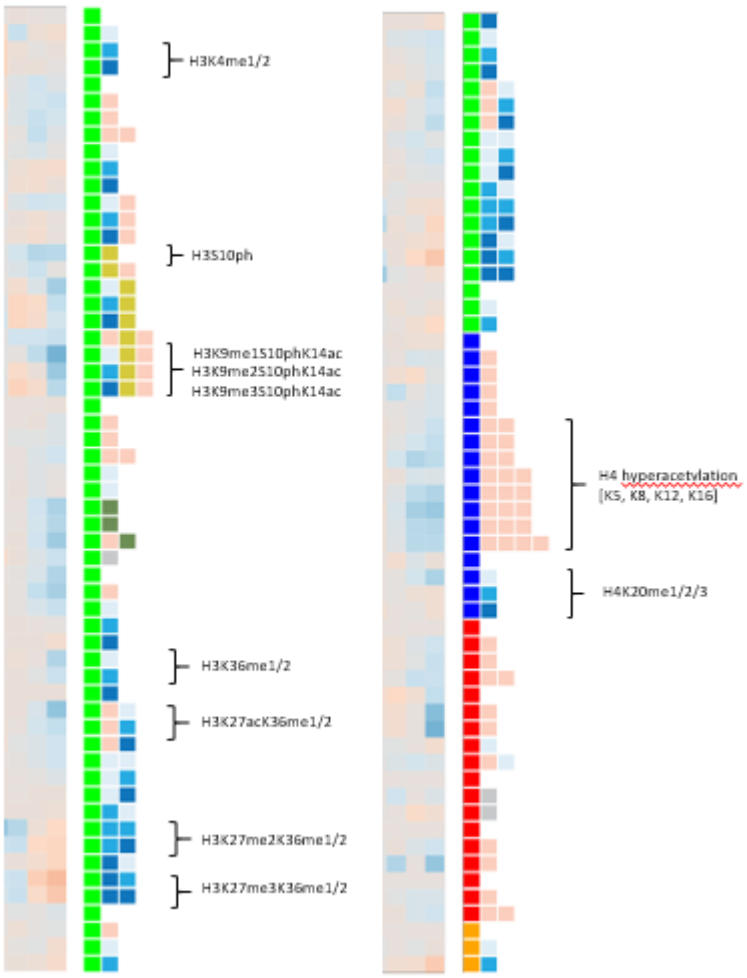

Figure 17: Several off-target effects induced by GSK-J4 treatment.

Figure 19 shows the tested lysine methytransferase inhibitors compared to GSK-J4. Regarding the combinatorial motifs the strongest increase was observed for the dimethylated H3K27 when H3K36 is dimethylated. Beside that, there is a slight increase in H3K27me2K36me3 as well as H3K27me3K36me1.

According to the study ´Inhibition of demethylases by GSK-J1/J4´ that has been published in Nature in 2014, Heinemann and his colleagues figure out that GSK-J4 lacks in specificity towards KDM6A/B. They also revealed an inhibition of H3K4 demethylases of the KDM5 family [37]. In contrast to that observation the results presented here does not show an increase in H3K4 methylation.

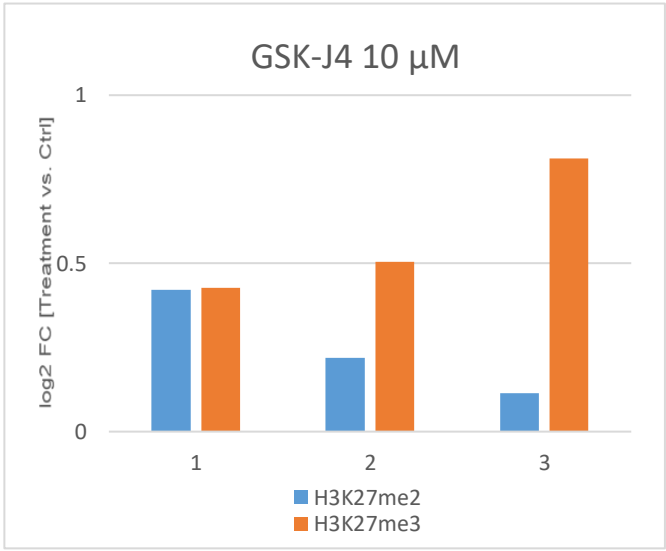

Figure 18: Change of abundance of di- and trimethylation of lysine 27 on histone 3 after GSK-J4 treatment.

Surprisingly treatment with GSK-J4 led to several off-target effects: Figure 17 shows a reduction in H4 hyperacetylation that increases over time.

Furthermore, inhibitor-treatment caused a strong decrease in H3S10ph-containing histone PTM motifs that led to the assumption of an impaired cell proliferation. On the other hand, this observation together with an increased number of floating/dead cells in cell culture experiment, raises the question whether inhibitor doses were too high. This would cause cytotoxicity and the resulting experimental data could not be related to the cellular mode of action of GSK-J4.

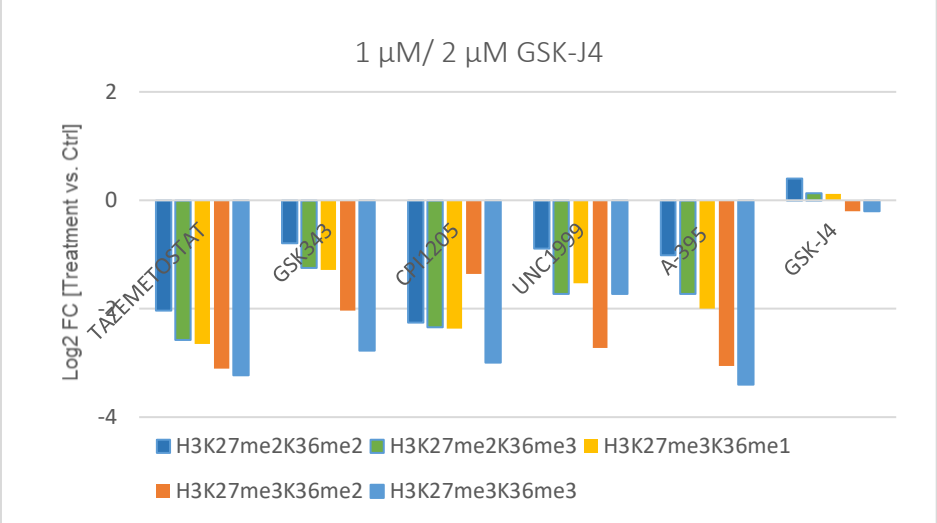

Figure 19: Comparison of PRC2 inhibitors versus PRC2 complex antagonist GSK-J4. An increase in methylation would be expected.

LSD1 inhibitors

Before the identification of the histone demethylase LSD1, histone methylation was considered to be irreversible [40]. LSD1 is responsible for demethylating the active H3K4me1/2. Due to the fact that the catalyzation of the process requires a protonated nitrogen as a hydrogen donor, the reaction only takes place on mono- and di-methylated lysines.

We tested two LSD1 inhibitors: ORY-1001 and GSK-LSD1. The inhibition of the demethylase LSD1 is expected to cause an increase in H3K4me2/3 but surprisingly a decrease in methylation was observed when cells where treated with ORY-1001 (Fig. 4). In case of the results received from GSK-LSD1 treatment, only a modest increase in the methylation level of lysine 4 on histone 3 was induced.

With our present knowledge about the mode of action of the demethylases, this observations remain inexplicable.

Furthermore, GSK-LSD1 treated cells show an increase in the trimethylation level of lysine 4 on histone 3. Interestingly, this increase was even stronger than the observed increase in H3K3me1/2 (Fig. 20).

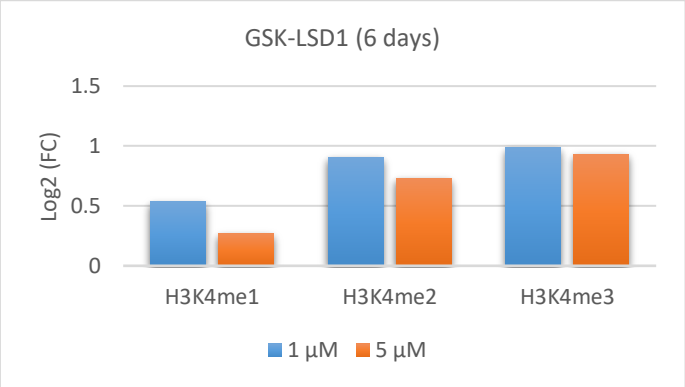

Figure 20: Log_2(FC) of mono-, di- & trimethylation of H3K4 compared to DMSO control after treatment with GSK-LSD1.

An explanation may be the downstream of H3K4 tri-methylating enzymes like Set7/9, MLL1-4 or SET1A induced by an indirect effct of the LSD1 treatment [41].

Regarding the suggested histone code hypothesis our data provide a decrease in H3K27me2/3K36me2/3 combinatorial motifs after 6 days of GSK-LSD1 treatment with no effect on the corresponding single posttranslational modification sites H3K27 and H3K36 (Fig. 21). However, the latter observation do not hold true at the higher dose of GSK-LSD1 treatment.

Summarising the observations, the need of further experiments particularly regarding optimal treatment dose is beyond debate.

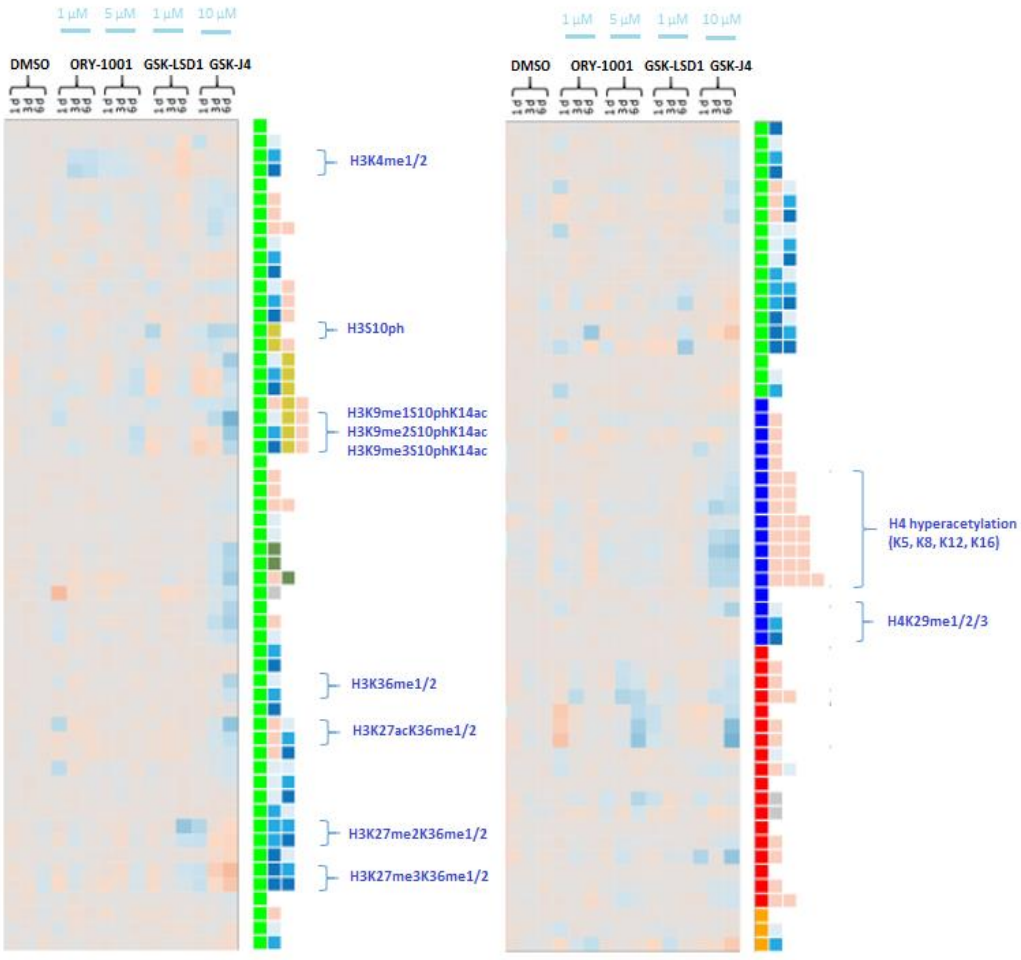

Figure 21: Response pattern induced by LSD1 inhibitors ORY-1001 and GSK-LSD1 & KDM6A/B inhibitor GSK-J4.

Characterization of novel inhibitor classes

Due to the need of new treatment strategies in regard of cancer, the investigation on the principle of action of proteins that are involved in posttranslational modifications are ongoing. The SGC (Structural Genomics Consortium) acts as the leading institution in respect of research and development of novel chemical probes.

In close collaboration they provided a variety of new KDM inhibitors to examine their effects on the global histone modification pattern.

Our aim was to investigate and collect data about their cellular mode of action using the epi-proteomic approach described earlier. These inhibitors targeting either the demethylating enzymes KDM2A, KDM5B, KDM6B or KDM4B. Moreover, we received compounds of the KDOPZ and KDOPP family of KDM5B inhibitors. Due to their covalent binding affinity to their target enzymes, they are of particular interest displaying a new chemotype of small molecule inhibitors.

Treatment of HeLa cells was performed in duplicates and using 3 µM of each inhibitor. As a negative control cells were treated with 0.2% DMSO. On the background of the previous experiments we decided to determine the effects using just one timepoint (3 d).

Having a look at the heatmap (Fig. 22) there are some interesting effects: surprisingly, the majority of the inhibitors show weak or even no effect towards their suggested primary target site which indicates an overall low specificity.

Table 1 shows the specificity scores for the new KDM inhibitor panel: the score indicates the effect of the inhibitor to it´s main target

Compound	Target site	Specificity (main + related)	Specificity (main)
KDOBA00072a	KDM6B	1.00	0.40
KDOBA00073a	KDM6B	0.93	0.47
KDOBA00086a	KDM6B	0.84	0.41
KDOBA00097a	KDM6B	1.25	0.27
KDOBA00075a	KDM6B	0.79	0.55
KDOPZ-48a	KDM5B	-	1.01
KDOPP-68a	KDM5B	-	2.00
KDOPZ-32	KDM5B	-	5.81
KDOPZ-50	KDM5B	-	1.43
KDOAM-25	KDM5B	-	2.23
KDOAM-21	KDM5B	-	4.64
CCT366629	KDM4B/ KDM5B	-	3.44
CCT365599	KDM4B/ KDM5B	-	1.76
KDOOA012000	KDM2A	1.03	0.30
KDOOA012001	KDM2A	1.29	1.02
KDOOA012002	KDM2A	1.01	0.53
KDOIN15	KDM2A	0.96	0.27

Table 1 : Table showing the specificity scores for the new KDM inhibitors.

compared to the average effectacross all quantified modifications. Therefore, the higher the score the stronger the effect.

Comparing the specificity of the novel compounds in regard of their main target, the most specific one belongs to the inhibitors targeting KDM5B (Table 1). Their scores ranging from 1.01 for KDOPZ-48a up to 5.81 for KDOPZ-32. With that score, KDOPZ-32 is the most specific inhibitor in this panel of new compounds. Although that increase in specificity is mostly caused by low overall effects, rather than a high potency in effecting H3K4me2/3 level.

Figure 22: Heatmap generated as the response pattern of modification-changes induced by the panel of novel compounds.

In order of the most potent compound the inhibitor KDOAM-21, which is also a member of the KDM5B inhibitor class, shows the greatest effect in inhibiting it´s main target. The trimethylation of H3K4 was 4-fold increased upon treatment (Fig. 23).

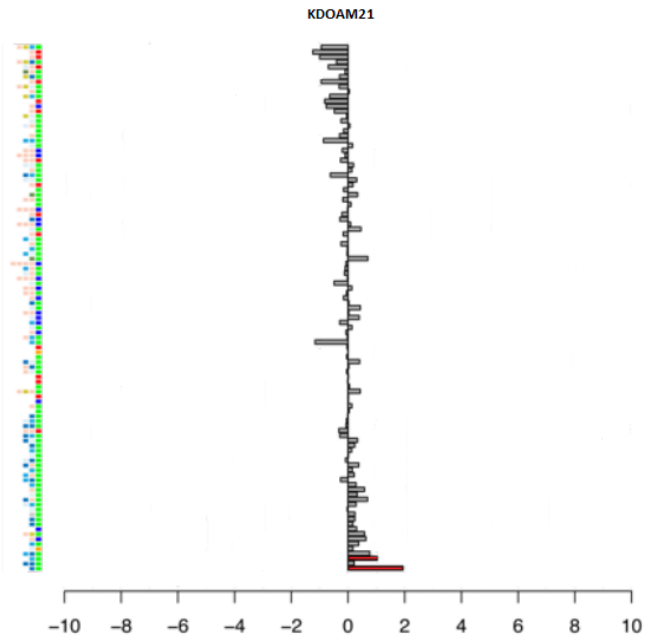

Neither the KDM2A/FBXL11 inhibitors nor the KDM5B and KDM4B/5B compounds showed a response in respect of their suggested main targets. Rather than affecting H3K36me1/2 (KDM2A) or H3K9me1/2 (KDM4B) an increase in H3K4me2/3 revealed- except for CCT365599 (Fig. 24). This target has only been expected for the KDM5B family of inhibitors [42].

Figure 23: KDM5B inhibitor KDOAM21 is the most potent compound in the panel of novel inhibitors. Red bars indicate the expected main target (H3K4me3).

Compared to the other compound families, the KDM6B inhibiting KDOBA series show a broad ranged response pattern. In regard of their target site H3K27me2/3, the low specificity is probably caused by global off-target effects.

Noteworthy is the high similarity to the GSK-J4 treatment pattern, which lead to the assumption that the cellular response is caused by cytotoxic effects.

Further experiments will be necessary to get knowledge in regard of the optimal treatment dose, taking into account that recent data suggest an effective concentration far below 1 µM [37, 43, 44].

Summarizing the obtained data of the novel compound panel, there are a lot of dissimilarities to previous findings assuming high inhibitor specificities in cellular assays [43]. On the other hands, this discrepancies are maybe owed to the different investigation methods.

Determination of inhibitor-induced effects on patient-derived Glioblastoma cell lines

Patient-derived Glioblastoma cell lines are used to study the several aspects of the disease in vitro and in vivo. There are two seperate classes: long-term cell lines and glioma initiating cells (GIC) that are also termed as glioma stem cells (GSC). The long-term cell lines grow as adherent cells in standard DMEM medium whereas the GSC need stem cell conditions. They grow in Neurobasal medium where growth factor and antibiotics has been added.

Beside the investigation of the molecular mode of action of inhibitors targeting PTMs modifying proteins in HeLa cells, we wanted to analyze if it´s possible to reduce GBM cell growth in vitro via inhibition of these enzymes.

The previous described mass-sprectrometry approach was applied to determine the effects of 40 inhibitors provided by the SGC (Table S 1). Our goal was to determine the effects of these compounds in a panel of 14 GBM cell lines (Fig. 24, left). To gather information regarding cell growth and cell viability in vitro, cells were treated in triplicates with 0.25, 1, 2.5 and 10 µM for six to eight days.
After the treatment an MTT assay was performed. The concept of an MTT assay is the chemical reduction of the yellow MTT (4-4,5-Dimethylthiazol-2-yl)-2,5-diphenyltreatrazolium bromide to purple formazan in the mitochondria of living cells. The accumulation of formazan in cells can then be determined by measuring the absorbance at 570 nm via a spectrophotometer, revealing information about cell viability.

By using a dilution series, we were able to get information about the dose-response effects for each inibitor in every cell line and, moreover, it was possible to determine the IC_{50} value (Fig. 24, right). This value is the inhibitor concentration that is required to reduce viable cells by 50%.

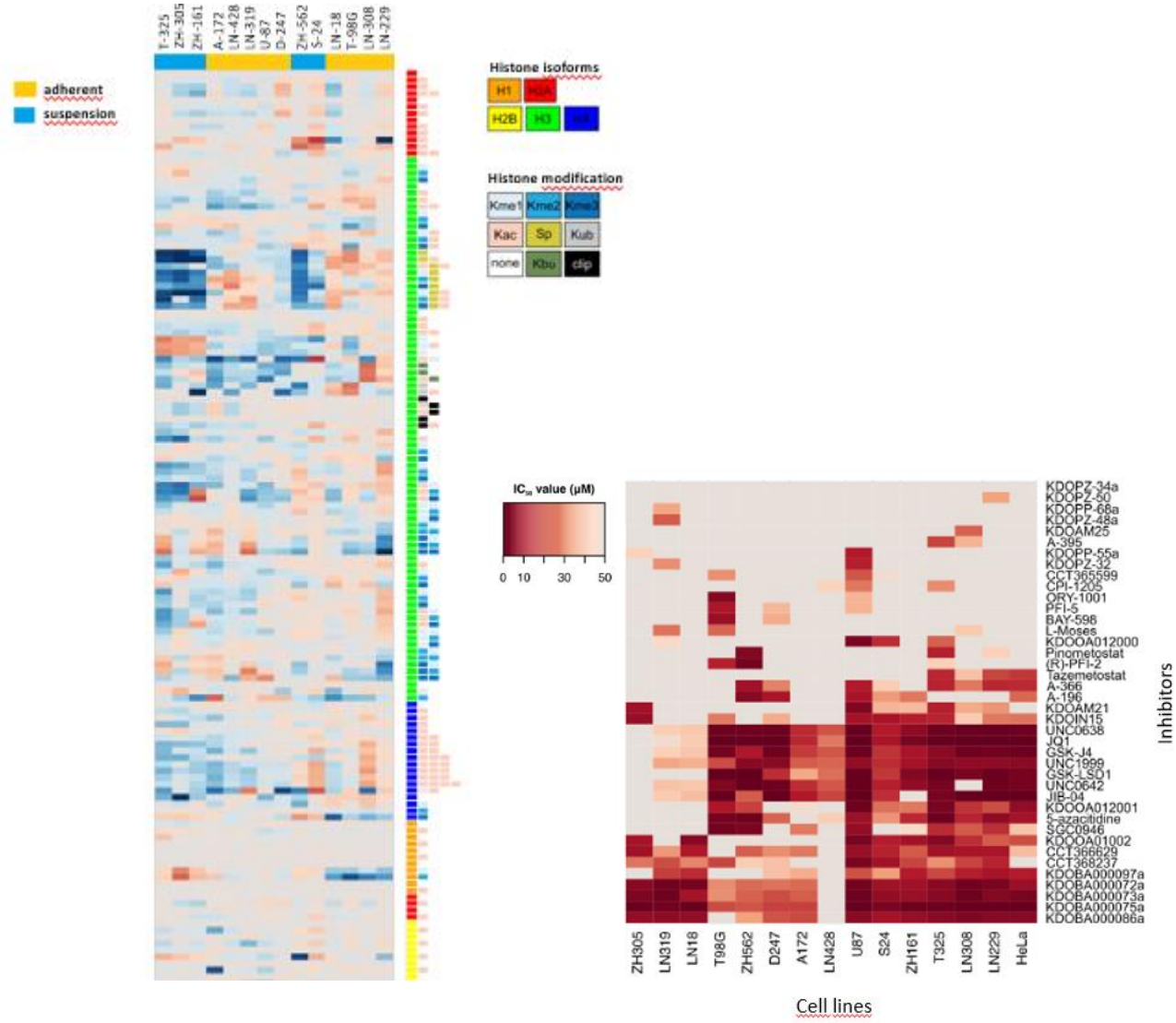

Figure 24: Left picture: Baseline histone PTM profile of 14 GBM cell lines. Abundance of the motifs is determined as the log_2 fold-change versus the average abundance across all cell lines. Right picture shows the response pattern of the IC_{50} value-experiment.

The most effective inhibitor were the ones from the KDOBA series inhibiting KDM6A/B (Fig. 24, right). Since the data reveals that inhibitors targeting the same protein (UNC1999, Tazemetostat, A395) do not automatically cause the same effects across cell lines, we quantified the cell cycle phase distribution as well as apoptotic stages via flow cytometry. By using this technology we aimed to gather additional information about the inhibitors mode of action.

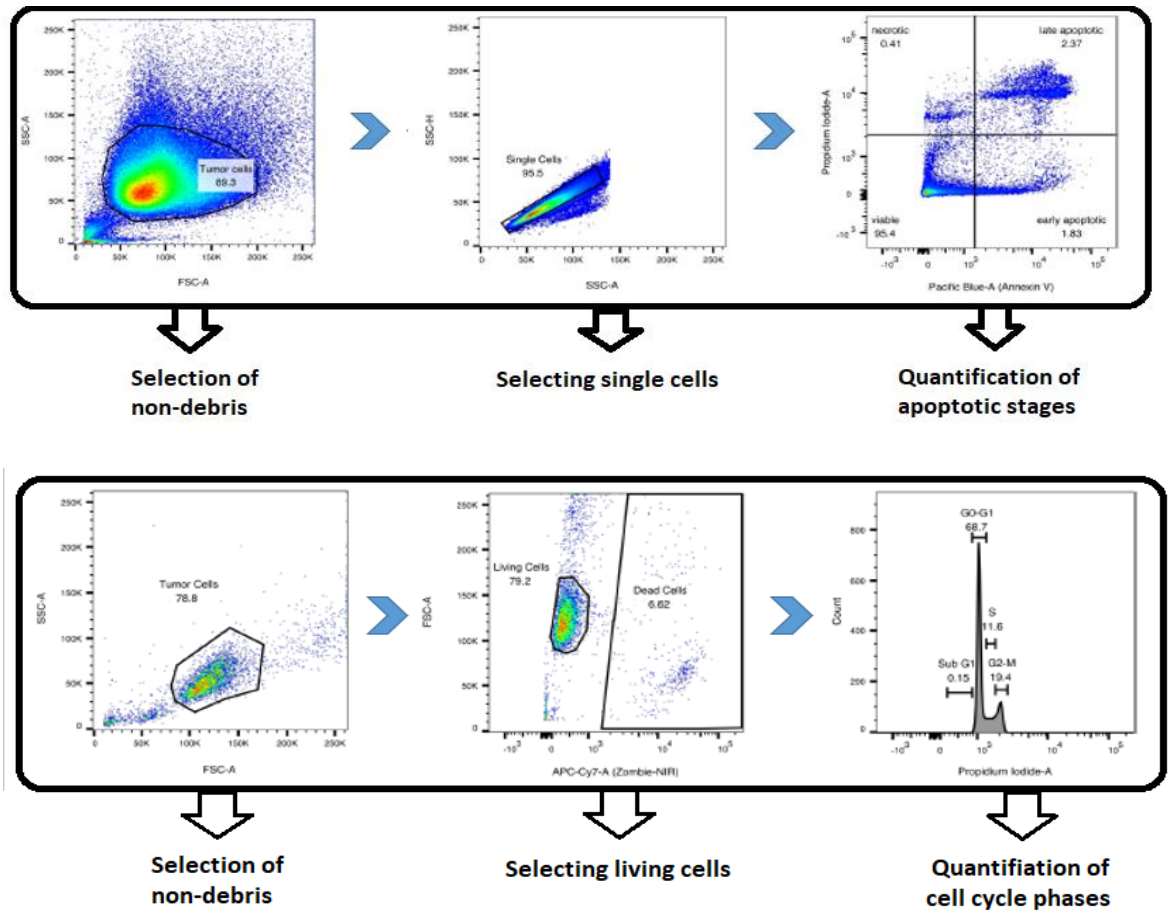

Figure 25: Workflow of the data analysis from the flow cytometry-based validation assay. Upper figure shows the gating process for the Annexin V/PI analysis (apoptosis). Lower picture displays selection of tumor cell population as well as living cells to determine the cell cycle phases.

Cell cycle quantification was done only on the basis of pre-gated „living“ cells based on life/dead staining (Fig. 25).

Quantification of cell cycle distribution and apoptotic stages were performed for selected inhibitors in a subset of three adherent and three suspension cell lines.

Representatively for all cell lines LN229 and T-325 show an enormous reduce of viable cells after treatment with GSK-J4 and KDOBA000075a while increasing the number of late apoptotic cells (Fig. 26). In most of the cases, the reduction was so strong that an association to the different cell cycle phases was impossible. As a result most remaining cells were classified as sub-G1.

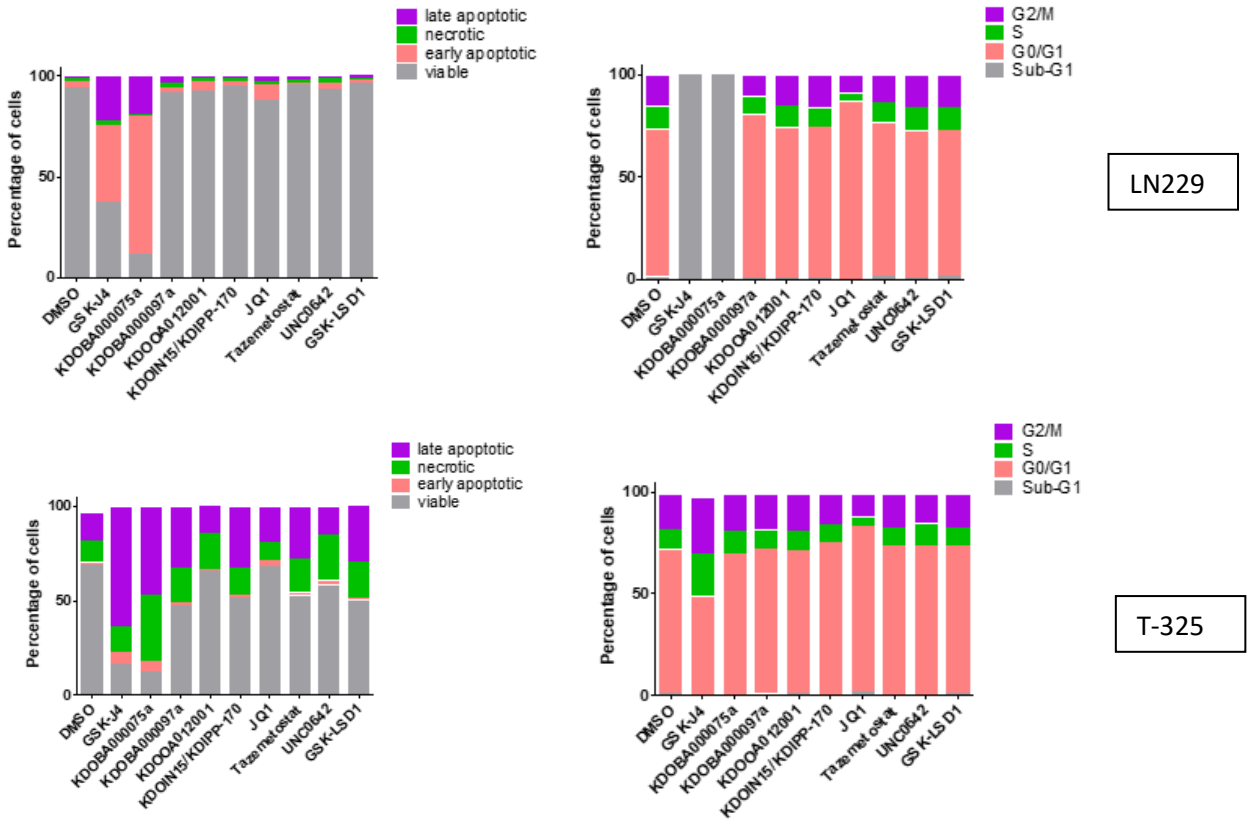

Figure 26: Adherent Glioblastoma cell line LN229 and suspension cell line T-325 representatively displayed for the results received from the flow cytometry-based validation assay. Cells were treated either with 1 µM (Tazemetostat, UNC0642, JQ1, GSK-LSD1) or 5 µM for 6 days. Left: Annexin V/PI (Apoptosis) experiment. Right: Cell cycle analysis

For T-325 cell cycle analysis revealed an increase in G2/M phase cells after treatment with GSK-J4. However, that increase is based at the expense of G0/G1 cells (Fig. 26).

Interestingly, KDOBA000075a evoked such an effect only in ZH-161 which is contradictory to an observed viability defect in T-325 when treated with this compound.

For a comprehensive prediciton regarding the inhibitor´s mode of action cell line-specific differences are too strong. For example, treatment with JQ1 caused different responses, like G0/G1 arrest in LN-229 or a G2/M phase cell gain in LN-319.

All in all, inhibitor treatment appeared to be more effective in glioma initiating cell than in glioma stem cells.

Conclusion

The aim and goal of this thesis was to investigate on the cellular mode of action of an inhibitor panel targeting different PTM modifying enzymes. In order to generate qualitatively high informations we used a newly mass-spectrometry based approach. For the reliability of the method we performed the experiments based on different concentrations, treatment durations as well as various inhibitors targeting the same protein.

Our first approach was to determine the post-translational modification pattern of HeLa cells after treatment with several inhibitors targeting epigenetically modifying proteins. For that purpose, the SGC provided a broad panel of inhibitors that are already in clinical use or even in clinical trials. Despite them, some novel compounds were investigated.

The analysis of the received data brought several differences in inhibitor specificities to light: some of the compounds, for example inhibitors targeting H3K79 methyltransferase DOT1L, are very specific. On the other hand, especially the treatment with the novel compounds, caused a lot of off-target effects which makes it hard to draw conclusions regarding their expected main target site.

As a second application we used the new mass-spectrometry based approach to examine the molecular effects of the inhibitors in a panel of 14 GBM cell lines. Among obtaining the baseline histone PTM profil of the cell lines, we were able to determine the IC_{50} value for each cell line and inhibitor. However, the performed flow-cytometry assay, to validate the received data, showed some irregularities. Thus highlighting a disadvantage of the new approach: for a better outcome it will be indispensable to gather more information regarding optimal treatment time for each compound.

Another crucial point is the seeding density, which limits the application of the technology in respect of using several different cell lines in one experiment.

In regard of the data analysis, today´s major challenge is not to generate big dataset´s but to analyse them accurately. Although the application of iRT spike-ins and synthetic reference peptides took place, a manually performed curation of peaks from the chromatogram was indispensable.

Concluding, this new mass-spectrometry approach not only lower the costs and impair the time management compared to the antibody-based methods that were used so far. But it allows to get information regarding PTM changes across several motifs in one experiment. Combined with standard biochemical assay the new technology provides an improvement and a great opportunity in respect of a better understanding of epigenetic modifiers and the cellular responses.

Supplementary

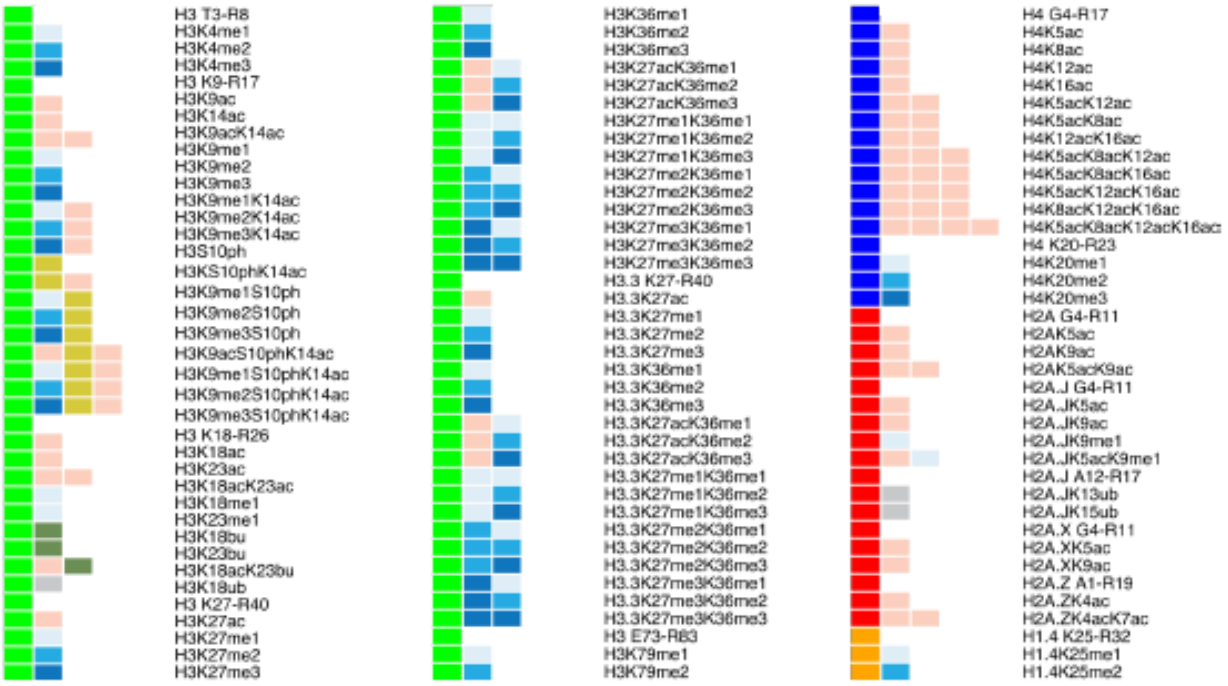

Figure S 1: Histone PTM color code annotation for the 114 motifs quantified in the experiment to characterize epigenetic inhibitors in HeLa cells.

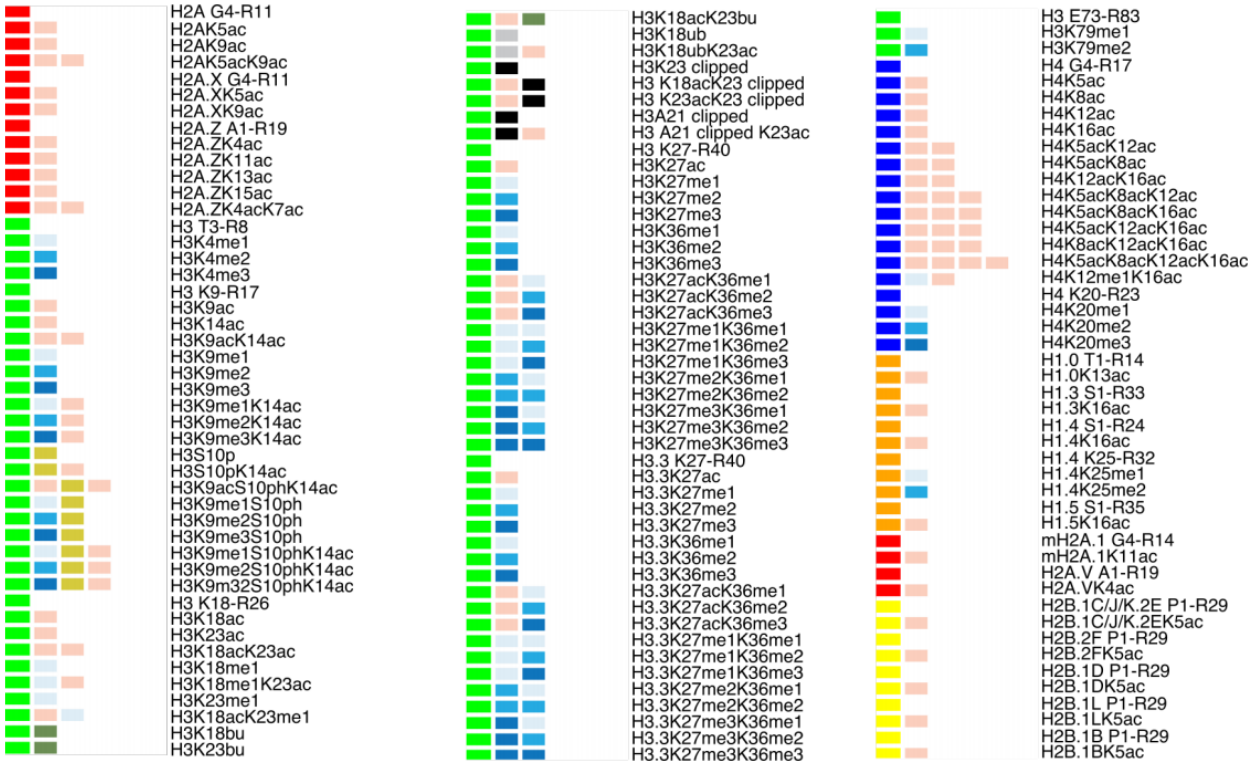

Figure S 2: Histone PTM color code annotation for the GBM baseline measurement.

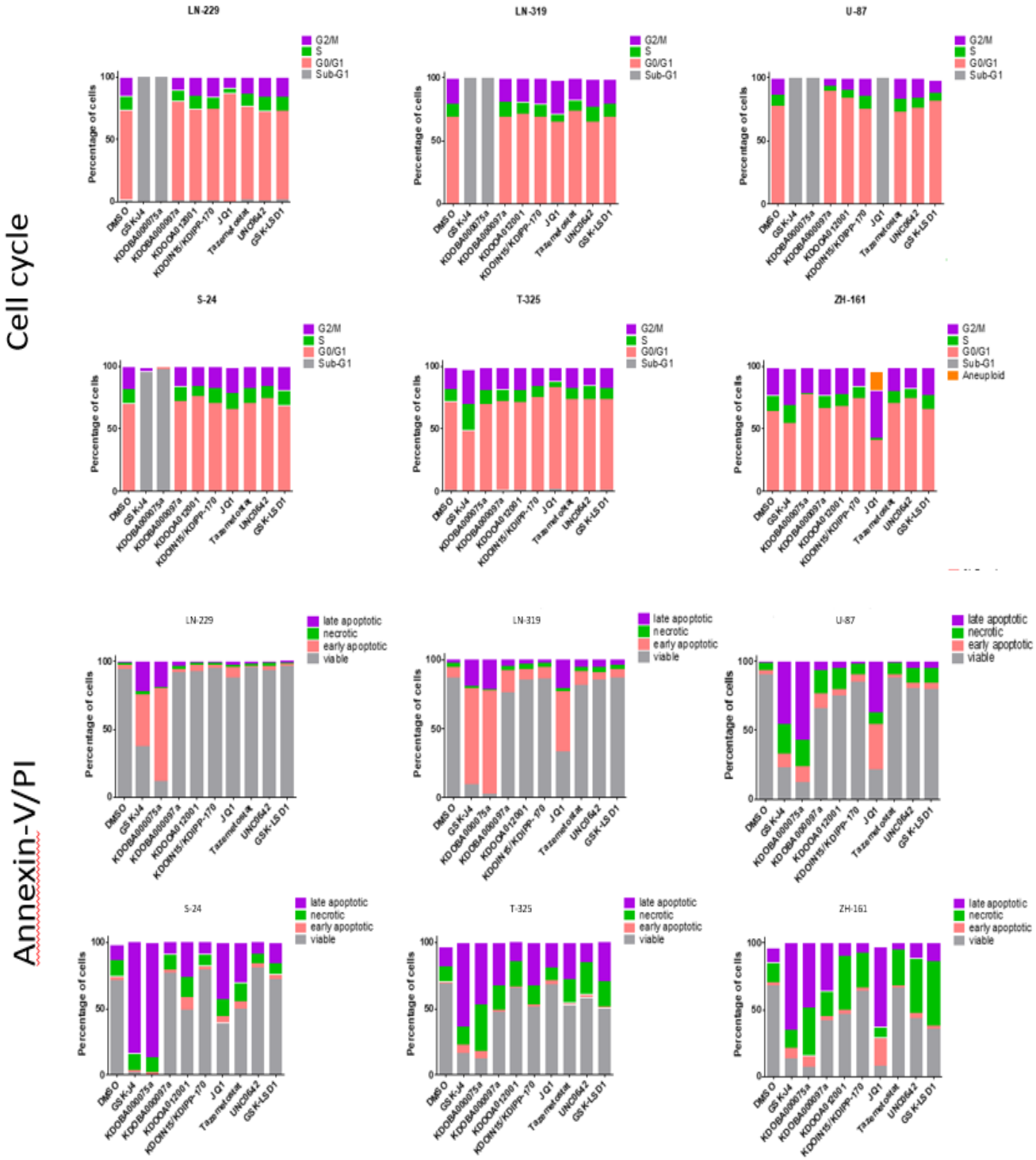

Figure S 3: Dataset of the flow-cytometry assay for the identification of the cell cycle phases.

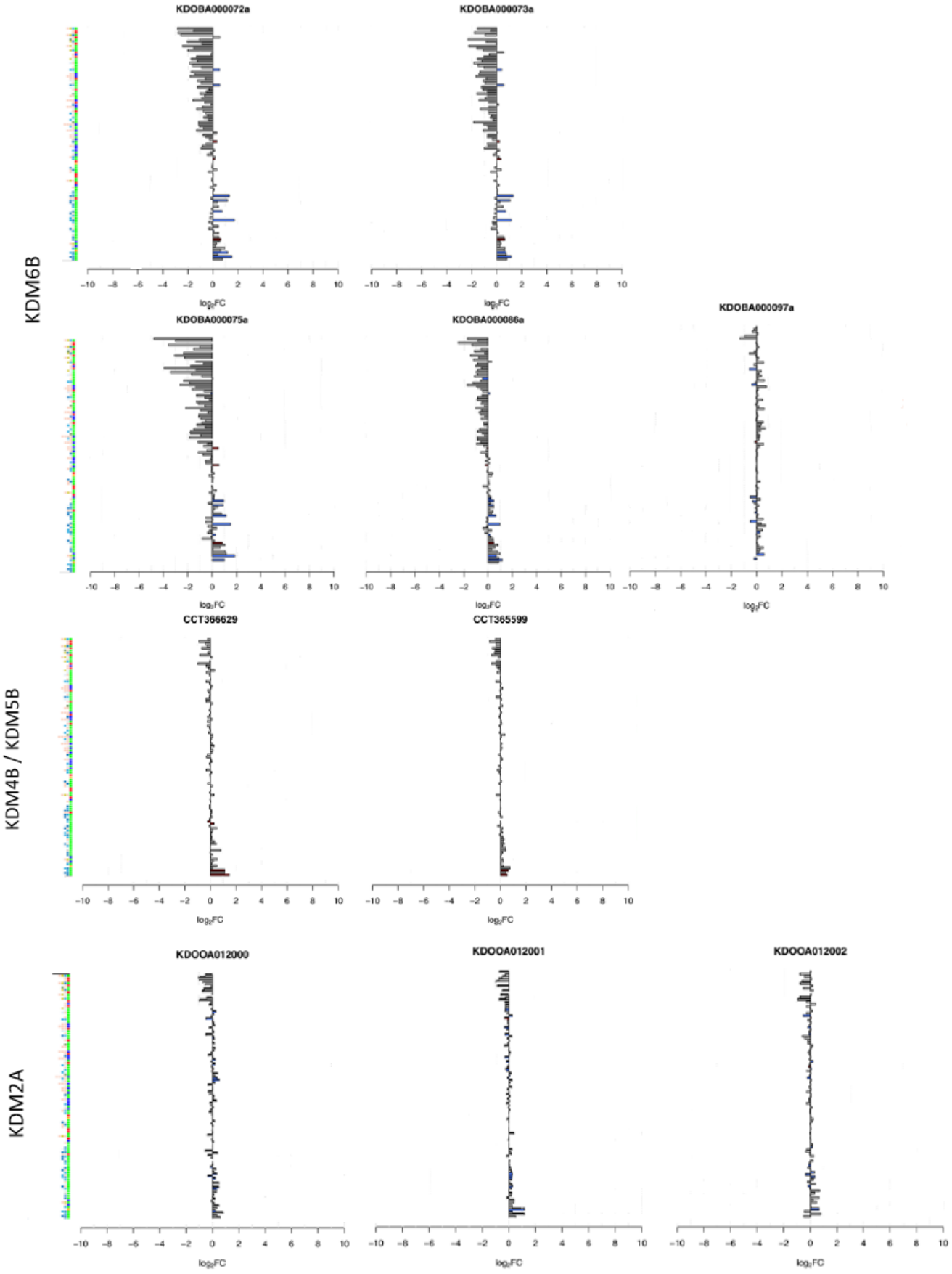

Figure S 4: Fingerplots displaying the response patterns of the novel inhibitor panel. Vertical axis: All quantified histone PTM motifs. Horizontal axis: log_2(FC) versus DMSO controls.

Compound	Target Enzyme	Enzyme Function	Histone Motif	Publication Status
JQ1	Bromo-i	-	-	published
UNC1999	EZH2/EZH1	Methyltransferase	H3K27me2/3	Published
A395	EED	Methyltransferase	H3K27me2/3	Published
CPI1205	EZH2	Methyltransferase	H3K27me2/3	Published
A366	G9a/GLP	Methyltransferase	H3K9me1/2	Published
UNC0642	G9a/GLP	Methyltransferase	H3K9me1/2	Published
UNC0638	G9a/GLP	Methyltransferase	H3K9me1/2	Published
SGC0946	DOT1L	Methyltransferase	H3K79me	Published
5´-azacitidine	DNMT1/2, RRM2	Methyltransferase	-	Published
A196	SUV420H1/2	Methyltransferase	H4K20me2	Published
GSK-LSD1	LSD1	Demethylase	H3K4me2/3	Published
ORY-1001	LSD1/KDM1A	Demethylase	H3K4me2/3	Published
KDOOA012000	FBXL11A	Demethylase	H3K36me	unpublished
KDOOA012001	FBXL11A	Demethylase	H3K36me	Unpublished
KDOOA012002	FBXL11A	Demethylase	H3K36me	Unpublished
CCT366629	JARID1B/JMJD2B	Demethylase	H3K4me/H3K9me	Unpublished
CCT365599	JARID1B/JMJD2B	Demethylase	H3K4me/H3K9me	Published
KDOPZ-34a	JARID1B	Demethylase	H3K4me	Unpublished
KDOPZ-48a	JARID1B	Demethylase	H3K4me	Unpublished
KDOPP-55a	JARID1B	Demethylase	H3K4me	Unpublished
KDOPP-68a	JARID1B	Demethylase	H3K4me	Unpublished
GSK-J4	KDM6	Demethylase	H3K27me	published
KDOBA000072a	KDM6	Demethylase	H3K27me	Unpublished
KDOBA000073a	KDM6	Demethylase	H3K27me	Unpublished
KDOBA000075a	KDM6	Demethylase	H3K27me	Unpublished
KDOBA000086a	KDM6	Demethylase	H3K27me	Unpublished
KDOBA000097a	KDM6	Demethylase	H3K27me	unpublished
BAY598	SMYD2	Methyl transferase /Demethylase	H3K4me/H3K36me2	published
PFI5	SMYD2	Methyl transferase /Demethylase	H3K4me/H3K36me2	published
GSK343	EZH2	Methyltransferase	H3K27me2/3	published
JIB04	JARID1A, JMJD2A, JMJD3	Demethylase		published
PFI2	SETD7	Methyltransferase	H3K4me1	published
Pinometostat	DOT1L	Methyltransferase	H3K79me1/2	published
Tazemetostat	EZH2	Methyltransferase	H3K27me2/3	published
CCT368237	KDM4	Demethylase	H3K9	unpublished
KDOPZ-32	JARID1B/KDM5B	Demethylase	H3K4	unpublished
KDOPZ-50	JARID1B/KDM5B	Demethylase	H3K4	Unpublished
KDOAM-25	JARID1B/KDM5B	Demethylase	H3K4	published
KDOAM-21	JARID1B/KDM5B	Demethylase	H3K4	published
KDOIN-15	FBXL11/KDM2A	Demethylase	H3K36	published

Table S 1: List of all inhibitors characterized by histone epi-proteomics.

References

[1] Rothbart, S.B., Dickson, B.M., B.M., Raab, J.R., Grzybowski, A.T., Krajewski, K., Guo, A.H., Shanle, E.K., Josefowicz, S.Z., Fuchs, S.M., Allis, C.D., *et al.* (2015). An Interactive Database for the Assessment of Histone Antibody Specificity. Mol Cell *59*, 502-511.

[2] Martin C., Zhang Y., (2005). The diverse functions of histone lysine methylation. Nat Rev Mol Cell Biol *6*, 838-849.

[3] Shilatifard A. (2006). Chromatin modifications by methylation and ubiquination: implications in the regulation of gene expression. Annu Rev Biochem *75*, 243-269.

[4] Jenuwein T., Allis C.D., (2001). Translating the histone code. Science *293*, 1074-1080.

[5] Cheung P., Tanner K.G., Cheung W.L., Sassone-Corsi P., Denu J.M., Allis C.D., (2000). Synergistic coupling of histone H3 phosphorylation and acetylation in response to epidermal growth factor stimulation. Mol Cell *5*, 905-915.

[6] Fischle W., Wang Y., Allis C.D., (2003). Histone and chromatin cross-talk. Curr Opin Cell Biol *15*, 172-183.

[7] Schworer, S., Becker, F., Feller, C., Baig, A.H., Kober, U., Henze, H., Kraus, J.M., Xin, B., Lechel, A., Lipka, D.B.*, et al.* (2016). Epigenetic stress responses induce muscle stemcell ageing by Hoxa9 developmental signals. Nature *540*, 428-432.

[8] Filippakopoulos P., Picaud S., Mangos M., Keates T., Lambert J.P., Barsyte-Lovejoy D., Felletar I., Volkmer R., Müller S., Pawson T., Gingras A.C., Arrowsmith C.H., Knapp S., (2012). Histone recognition and large-scale structural analysis of the human bromodomain family. Cell *149*, 214-231.

[9] Portela A., Esteller M., (2010). Epigenetic modifications and human disease. Nat Biotechnol *28*, 1057-1068.

[10] Sturm D., Witt H., Hovestadt V., Khuong-Quang D.A., Jones D.T.W., Konerman C., Pfaff E., Tönjes M., Sill M., Bender S., (2012). Hotspot mutations in H3F3A and IDH1 define distinct epigenetic and biological subgroups of glioblastoma. Cancer Cell *22*, 425-437.

[11] Gusyatiner O., Hegi M.E. (2018). Glioma epigenetics: From subclassification to novel treatment options. Semin Cancer Biol *51*, 50-58.

[12] Capper D., Jones D.T.W., Sill M., Hovestadt V., Schrimpf D., Sturm D., Koelsche C., Sahm F., Chavez L., Reuss D.E.*, et al.* (2018). DNA methylation-based classification of central nervous system tumours. Nature *555*, 469-474.

[13] Flavahan W.A., Drier Y., Liau B.B., Gillespie S.M., Venteicher A.S., Stemmer-Rachamimov A.O., Suva M.L., and Bernstein B.E. (2016). Insulator dysfunction and oncogene activation in IDH mutant gliomas. Nature *529*, 110-114.

[14] Helin K., Dhanak D., (2013). Chromatin proteins and modifications as drug targets. Nature *502*, 480-488.

[15] Kleer C.G., Cao Q., Varambally S., Shen R., Ota I., Tomlins S.A., Ghosh D., Sewalt R.G., Otte A.P., Hayes D.F., (2003). EZH2 is a marker of aggressive breast cancer and promotes neoplastic transformation of breast epithelial cells. Proc Natl Acad Sci USA *100*, 11606-11611.

[16] Wagener N., Macher-Goeppinger S., Pritsch M., Hüsing J., Hoppe-Seyler K., Schirmacher P., Pfitzenmaier J., Haferkamp A., Hoppe-Seyler F., Hohenfellner M., (2010). Enhancer of zeste homolog 2 (EZH2) expression is an independent prognostic factor in renal cell carcinoma. BMC Cancer *10*, 524.

[17] Takawa M., Masuda K., Kunizaki M., Daigo Y., Takagi K., Iwai Y., Cho H.S., Toyokawa G., Yamane Y., Maejima K., *et al.* (2011). Validation of the histone methyltransferase EZH2 as a therapeutic target for various types of human cancer and as a prognostic marker. Cancer Sci *102*, 1298-1305.

[18] Bannister A.J., Kouzarides T., (2011). Regulation of chromatin by histone modifications. Cell Res *21*, 381-395.

[19] Kouzarides T. (2007). Chromatin modifications and their function. Cell *128*, 693-705.

[20] He Y., Selvaraju S., Curtin M.L., Jakob C.G., Zhu H., Comess K.M., Shaw B., The J., Lima-Fernandes E., Szewczyk M.M., *et al*. (2017). The EED protein-protein interaction inhibitor A-395 inactivates the PRC2 complex. Nat Chem Biol *13*, 389-395.

[21] Verma S.K., Tian X., LaFrance L.V., Duquenne C., Suarez D.P., Newlander K.A., Romeril S.P., Burgess J.L., Grant S.W., Brackley J.A., *et al*. (2012). Identification of Potent, Selective, Cell-Active Inhibitors of the histone lysine Methyltransferase EZH2. ACS Med Chem Lett *3*, 1091-1096.

[22] Simon J.A., Kingston R.E., (2013). Occupying chromatin: Polycomb mechanisms for getting to genomic targets, stoppig transcriptional traffic, and staying put. Mol Cell *7*, 808-824.

[23] Huang J., Dorsey J., Chuikov S., Perez-Burgos L., Zhang X., Jenuwein T., Reinberg D., Berger S.L., (2010). G9a and GLP methylate lysine 373 in the tumor suppressor p53. J Biol Chem *285*, 9636-9641.

[24] Tachibana M., Sugimoto K., Nozaki M., Ueda J., Ohta T., Ohki M., Fukuda M., Takeda N., Niida H., Kato H., Shinkai Y., (2002). G9a histone methyltransferase plays a dominant role in euchromatic histone H3 lysine 9 methylation and is essential for early embryogenesis. Genes Dev *16*, 1779-1791.

[25] Kondo Y., Shen L., Suzuki S., Kurokawa T., Masuko K., Tanaka Y., Kato H., Mizuno Y., Yokoe M., Sugauchi F., (2007). Alterations of DNA methylation and histone modifications contribute to gene silencing in hepatocellular carcinomas. Hepatol Res *37*, 974-983.

[26] Huang T., Zhang P., Li W., Zhao T., Zhang Z., Chen S., Yang Y., Feng Y., Li F., Liu S.X., *et al.* (2017). G9a promotes tumor cell growth and invasion by silencing CASP1 in non-small-cell lung cancer cells. Cell Death Dis *8*, 2726.

[27] Wu H., Chen X., Xiong J., Li Y., Li H., Ding X., Liu S., Chen S., Gao S., Zhu B., (2011). Histone methyltransferase G9a contributes to H3K27 methylation in vivo. Cell Res *21*, 365-367.

[28] Weiss T., Hergeth S., Zeissler U., Izzo A., Tropberger P., Zee B.M., Dundr M., Garcia B.A., Daujat S., Schneider R. (2010). Histone H1 variant-specific lysine methylation by G9a/KMT1C and Glp1/KMT1D. Epigenetics Chromatin *3*, 7.

[29] Trojer P., Zhang J., Yonezawa M., Schmidt A., Zheng H., Jenuwein T., Reinberg D., (2009). Dynamic Histone H1 Isotype 4 Methylation and Demethylation by Histone Lysine Methyltransferase G9a/KMT1C and the Jumonji Domain-containing JMJD2/KDM4 Proteins. J Biol Chem *284*, 8395-8405.

[30] Vedadi M., Barsyte-Lovejoy D., Liu F., Rival-Gervier S., Allali-Hassani A., Labrie V., Wigle T.J., Dimaggio P.A., Wasney G.A., Siarheyeva A.*, et al.* (2011). A chemical probe selectively inhibits G9a and GLP methyltransferase activity in cells. Nat Chem Biol *7*, 566-574.

[31] Liu F., Barsyte-Lovejoy D.A., Li F., Xiong Y., Korboukh V., Huang X.P., Allali-Hassani A., Janzen W.P., Roth B.L., Frye S.V., *et al.* (2013). Discovery of an in vivo chemical probe of the lysine methytransferases G9a and GLP. J Med Chem *56*, 8931-8942.

[32] Kim Y., Lee H.M., Xiong Y., Sciaky N., Hulbert S.W., Cao X., Everitt J.I., Jin J., Roth B.L., Jiang Y.H., (2017). Targeting the histone methyltransferase G9a activates imprinted genes and improves survival of a mouse model of Prader-Willi syndrome. Nat Med *23*, 213-222.

[33] Schotta G., Lachner M., Sarma K., Ebert A., Sengupta R., Reuter G., Reinberg D., Jenuwein T., (2004). A silencing pathway to induce H3-K9 and H4-K20trimethylation at constitutive heterochromatin. Genes Dev *18*, 1251-1262.

[34] Hergeth S.P., Schneider R., (2015). The H1 linker histones: multifunctional proteins beyond the nucleosomal core particle. EMBO Rep *16*, 1439-1453.

[35] Jacobs S.A., Taverna S.D., Zhang Y., Briggs S.D., Li J., Eissenberg J.C., Allis C.D., Khorasanizadeh S., (2001). Specificity of the HP1 chromo domain for the methylated N-terminus of histone H3. EMBO J *20*, 5232-5241.

[36] Wood K., Tellier M., Murphy S., (2018). DOT1L and H3K79 Methylation in Transcription and Genomic Stability. Biomolecules *8*, 11.

[37] Heinemann B., Nielsen J.M., Hudlebusch H.R., Lees M.J., Larsen D.V., Boesen T., Labelle M., Gerlach L.O., Birk P., Helin K., (2014). Inhibition of demethylases by GSK-J1/J4. Nature *514*, E1-2.

[38] Donas C., Carrasco M., Fritz M., Prado C., Tejon G., Osorio-Barrios F., Manriquez V., Reyes P., Pacheco R., RosaBono M., *et al*. (2016). The histone demethylase inhibitor GSK-J4 limits inflammation through the induction of a tolerogenic phenotype on DCs. J Autoimmun *75*, 105-117.

[39] Li Y., Zhang M., Sheng M., Zhang P., Chen Z., Xing W., Bai J., Cheng T., Yang F.C., Zhou Y., (2018). Therapeutic potential of GSK-J4, a histone demethylase KDM6B/JMJD3 inhibitor, for acute myeloid leukemia. J Cancer Res Clin Oncol *144*, 1065-1077.

[40] Shi Y., Lan F., Matson C., Mulligan P., Whetstine J.R., Cole P.A., Casero R.A., Shi Y. (2004). Histone demethylation mediated by the nuclear amine oxidase homolog LSD1. Cell *119*, 941-953.

[41] Ruthenburg A.J., Allis C.D., Wysocka J. (2007). Methylation of lysine 4 on histone H3: intricacy of writing and reading a single epigenetic mark. Mol Cell *25*, 15-30.

[42] Horton J.R., Engstrom A., Zoeller E.L., Liu X., Shanks J.R., Zhang X., Johns M.A., Vertino P.M., Fu H., Cheng X., (2016). Characterization of a Linked Jumonji Domain of the KDM5/JARID1 Family of Histone H3 Lysine 4 Demethylases. J Biol Chem *291*, 2631-2646.

[43] Hatch S.B., Yapp C., Montenegro R.C., Savitsky P., Gamble V., Tumber A., Ruda G.F., Bavetsias V., Fedorov O., Atrash B*., et al.* (2017). Assessing histone demethylase inhibitors in cells: lessons learned. Epigenetics Chromatin *10*, 9.

[44] Kruidenier L., Chung C.W., Cheng Z., Liddle J., Che K., Joberty G., Bantscheff M., Bountra C., Bridges A., Diallo H*., et al.* (2012). A selective jumonji H3K27 demethylase inhibitor modulates the proinflammatory macrophage response. Nature *488*, 404-408.

[45] Sawicka A., Seiser C., (2012). Histone H3 phosporylation- A versatile chromatin modification for different occasions. Biochimie *94*, 2193-2201.

Zusammenfassung

Genexpression und Chromatinstruktur in tierischen Zellen werden durch unterschiedlichste epigenetische Mechanismen wie zum Beispiel posttranslationalen Histonmodifikationen gesteuert. Veränderungen dieses Modifikationsmuster bildet die Ursache zahlreicher Erkrankungen. Aufgrunddessen wächst das Interesse die, der epigenetischen-Prozesse, zugrundeliegenden Mechanismen aufzudecken.

Bis heute bediente man sich bevorzugt antikörper-basierten Methoden wie zzum Beispiel dem Immunoblotting, Immunohistochemie oder dem Chromatin ImmunoPrecipitation DNA-Sequencing, um Veränderungen des Histonmodifikationsmusters aufzudecken. Das Hauptaugenmerk liegt hierbei vor allem auf Methylierungs-, Acetylierungs- und Phosphorylierungsreaktionen.

In Bezug auf die bis dato verwendeten experimentellen Methoden ist besonders der Umstand, dass es nur Antikörper im Hinblick auf bereits bekannte Histonmodifikationen gibt, limitierend [1].

Das Ziel dieses Projekts war die Identifikation der Veränderungen im Histonprofil unter Verwendung einer kürzlich entwickelten Methode, die auf massenspektrometrischen Messungen basiert. Untersucht wurde der Einfluss verschiedener Inhibitoren sowohl auf HeLa Zellen als auch auf Glioblastom-Zellen. Diese Inhibitoren hemmen die spezifischen Enzyme, die in epigenetische Prozesse eingebunden sind. Es wurden die Veränderungen von über 100 Histonmodifikationen quantifiziert.

Die so generierten Daten zeigen, dass diese neue Methode, vor allem in Kombination mit etablierten biologischen Untersuchungsansätzen, eine neue Strategie bilden, um den Zusammenhang zwischen epigenetischen Veränderungen und der Entwicklung verschiedenster Erkrankungen zu untersuchen.